Synthesis of Tellurene Nanorods: Exploring Optical and Dielectric Properties, and Sensitivity Towards H_2O_2 Sensing

A thesis submitted towards partial fulfilment of the requirements for the degree of:

MASTER OF TECHNOLOGY IN

NANOSCIENCE AND TECHNOLOGY

SUBMITTED BY:

ARNAB KUMAR SAHA

ROLL NO. :002230701008

EXAMINATION ROLL NO.:M4NST24008

REGISTRATION NO.: 156291 OF 2020-21

UNDER THE GUIDANCE OF

PROF. SOURAV SARKAR

SCHOOL OF MATERIALS SCIENCE AND NANOTECHNOLOGY JADAVPUR UNIVERSITY

KOLKATA – 700032

COURSE AFFILIATED TO

FACULTY OF INTERDISCIPLINARY STUDIES, LAW AND MANAGEMENT

JADAVPUR UNIVERSITY, KOLKATA, INDIA

2024

M.Tech (Nano Science and Technology)
Course affiliated to:
Faculty of Interdisciplinary Studies, Law and Management
Jadavpur University, Kolkata, India

CERTIFICATE OF RECOMMENDATION

This is in order to certify that the thesis entitled " Synthesis of Tellurene Nanorods: Exploring Optical and Dielectric Properties, and Sensitivity Towards H2O2 Sensing" is a legitimate work done by Arnab Kumar Saha, Roll No -002230701008, Reg No, 156291 of 2020-21 under our supervision and guidance for the purposes of fulfilling the requirement for the degree of Master of Technology in Nano Science and Nanotechnology in the School of Materials Science and Nanotechnology from the academic session 2022-2024.

_____

THESIS ADVISOR

Dr. Sourav Sarkar

School of Materials Science and NanotechnologyJadavpur University,
Kolkata-700 032

_____

DIRECTOR
Dr. Mahua Ghosh Chowdhury
School of Materials Science and NanotechnologyJadavpur University,
Kolkata-700 032

_____

DEAN

Faculty Council of Interdisciplinary Studies, Law and Management
Jadavpur University, Kolkata-700 032

M.Tech (Nano Science and Technology)
Course affiliated to:
Faculty of Interdisciplinary Studies, Law and Management
Jadavpur University, Kolkata, India

CERTIFICATE OF APPROVAL

I hereby endorse the foregoing thesis as an engineering study, conducted and presented in a manner satisfactory enough to justify its acceptance as an engineering study, in order to obtain the degree for which it has been submitted. This approval does not endorse or approve any statement made, opinion expressed or conclusion drawn therein, but merely approves the thesis for the purpose for which it has been submitted.

Committee of the final examination
for evaluation of the Thesis

_____
_____
_____
_____

DECLARATION OF ORIGINALITY AND COMPLIANCE OF ACADEMIC ETHICS

I hereby declare that this thesis contains a literature survey and original research work by the undersigned candidate for the Master of Technology (Nano Science and Technology) program during the academic year 2020-2022.

The information in this document has been gathered and presented according to academic standards and ethical conduct. I also declare that I have cited and referred to all materials and results that are not original to this work as required by these rules and conduct.

Name: **ARNAB KUMAR SAHA**

Roll Number: **M4NST24008**

Registration Number: **156291 of 2020-21**

Thesis Title: Study of Morphological and Optical property of Emerging 2D tellurene material

SIGNATURE **DATE**

Acknowledgement

The work described in this thesis entitled as “Study of Morphological and Optical property of Emerging 2D tellurene material” started in the ‘Nanoscience and Nano-technology laboratory’ and ‘Thin-films and Nano-technology Laboratory’ of Jadavpur University in November 2023 would not have been what it is today without the support of others. Foremost I would like to express my sincere gratitude to my advisors, Dr. Sourav Sarkar for the continuous support of my Master’s study and research, for his patience, motivation, enthusiasm and immense knowledge. His guidance helped me all the time and in writing of this thesis. I could not have imagined any better advisor and mentor for my Master’s thesis. I am grateful to you for guiding me during the entire course of research work with your valuable suggestions. Thank you also for the amicable environment conducive to extensive research work at Nano- Lab, in which you have welcomed me.

I am also indebted to Prof. Kalyan Kumar Chattopadhyay, Dr. Chandan Kumar Ghosh, and Dr. Mahua Ghosh Chowdhury for their valuable suggestions and criticism during the course of my MTech program. Their enthusiasm, encouragement, insightful comments and hard questions provided me a helpful and effective way of learning, which in turn inspired me to follow the research project with great strength.

I extend my heartiest thanks to my mentor Mr. Sk Najes Riaz to have guide me, motivate me, helped in allmy difficulties in this project and worked jointly to achieve what the project has turned out to be today.

My sincere thanks goes out to Koustav Samaddar, Gourav Payra, Sourav Ghosh, Kazi Wakar Hasan, who have helped me throughout my project work and provided me with their immense support with rich scientific ideas and encouragement to work hard.

A lot of gratitude towards my seniors, Manas Thakur, Souvik Poddar, Nabanita Sen, Suvra Pal, Kabir Khan to extend their helping hands to me whenever I needed, making my project a really fulfilling experience, and always making me feel a part of their family. I owe special thanks to my parents and classmates during this course work, for their constant support. All of them provided me with great support during my project, which I do not think I would have been able to complete otherwise. This gratitude is too small in front their great support.

Content

1. Introduction 9-13
   - Morphology 10
   - Te Rod 10
   - Te 2D Sheet 11
   - Te Quantum Dots 12
   - Motivation 13
   - Application 13
2. Instrumentation 17-39
   - Morphological Analysis 17
   - Optical Property Analysis 20
   - UV-VIS near Infrared Spectroscopy 20
   - Photoluminescence 24
   - X-Ray Diffraction 27
   - FTIR 30
   - Raman Spectroscopy 34
   - Literature Review 39
3. Experiments:
   - Synthesis of Samples 51
   - Material 52
   - Sample Peparatation 52
4. Result & Discussion 55-68
   - XRD 55
   - Fourier-transform infrared spectroscopy 58
   - Raman Spectroscopy 60
   - PL Spectrum 61
   - Dielectric Measurement &Analysis 62
   - Scanning Electron Microscope Analysis 68
   - Cyclic Voltammetry Analysis 68
5. Conclusion 73
6. References 74

Abstract

Tellurium nanorods (TeNRs) are the basis of a novel, inexpensive, non-enzymatic sensor for the analytical measurement of H2O2. An economically feasible electrochemical method was utilized to synthesize the non-enzymatic H2O2 sensor based on TeNRs. Research has been done on the impact of deposition potential on the electrochemical characterization, phase development, and morphology of nanostructured Te films. The nanostructured Te films on the GC surface were characterized by Raman, Uv-Vis Spectroscopy, X-ray diffraction, and field emission scanning electron microscopy. Cyclic voltammetry (CV) and chronoamperometry (CA) have been used to examine the electro-catalytic performance of the suggested TeNPs/GC sensor in phosphate buffer both in the presence and absence of H2O2. TeNRs/GC shown exceptional electro-catalytic activity towards H2O2 reduction when manufactured at an applied potential of -0.7V. With an outstanding amperometry response time of around 5 s, the sensor has exceptional selectivity and stability. The current investigation also shows that TeNPs/FTO is a potential sensing material that may be used to measure H2O2 in real-world samples.

Chapter - 1

Introduction

Introduction:

Since the beginning of human civilization, people have been deeply intrigued about energy. We have always relied on energy to survive in this wonderful world, from fire to electricity. Energy cannot be generated or destroyed; it can only be transformed into another form, as we learn later from the law of conservation of energy. Unknowingly, our forebears did the same. Our lives have been significantly improved by nanoelectronics technology, which is made possible by the sophisticated disciplines of the semiconductor industry. These days, people are attempting to improve performance and reduce the size of all those technological devices. Today's integrated circuit components, such as transistors and diodes, are built using a top-down approach and bottom-up approach. As Moore predicted in 1965, the size and cost of producing the fundamental transistor still halve every two years. It is anticipated that the 28 nm transistor size of today will drop to 14 nm in 2014–15 due to advancements in production technology alone. It is estimated that the underlying physical limits of this manufacturing process will prevent it from reaching lower sizes in ten to fifteen years. For complementing opto-electrical purposes, a bottom-up approach to circuit assembly employing atomic, single-molecule, carbon nanotube, quantum dot, or nanowire building blocks can be useful, but the same physical limits will apply. Another illustration would be the surface of a smaller object with a different electrical structure than the material in bulk. Additionally, a higher surface-to-volume ratio makes the nanostructure more sensitive to its environment, which might be advantageous for sensors or harmful for electrical or photonic transport, light generation, etc. They show promise not only for computation but also for chemical, biological, and medical detection, as well as connecting structures. Nanostructures can have very sensitive features to surface changes because of their large surface-to-volume ratio. It is evident that there is frequently no discernible difference between the domains of nanoscience and technology because they are so closely linked. Up until now, there have also been difficulties because standard planar fabrication technique would be limited as device shrinking demands even higher precision technology. Materials with one-dimensional (1D) nanostructures have made

it possible to overcome the difficulties. Worldwide, its potential for use in the electronics sector has sparked interest in numerous research labs.

Because of their remarkable dielectric qualities, insulators are employed in dielectric materials. The capacity of a dielectric to sustain an electrical field while releasing the least amount of energy as heat. A dielectric substance is more effective the smaller its dielectric loss (the percentage of energy wasted as heat). The dielectric constant, which measures how much a material concentrates the electrostatic lines of flux, is another factor to take into account. Most pure, dry gases, such as nitrogen and helium, as well as a perfect vacuum are examples of substances with a low dielectric constant. Paper, mica, polyethylene, glass, ceramics, and distilled water are examples of materials with modest dielectric constants. Metal oxides, in general, have high dielectric constants. A substance that effectively supports electrostatic fields but conducts electricity poorly is known as a dielectric material. Should the current flowing between the opposing electric charge poles be An electrostatic field can store energy if it is minimized and the electrostatic lines of flux remain unhindered. Capacitors can benefit from this feature, particularly at radio frequencies. Radio-frequency transmission lines are another application for dielectric materials.
Each material possesses a distinct set of electrical properties that rely on its dielectric qualities. Precise assessments of these characteristics can furnish researchers and providing engineers with important information to monitor a production process for better quality control or to correctly incorporate the material into its intended application for more robust designs.

Morphology:

Te Rod:

As wireless electronic gadgets or communication equipment have grown rapidly, serious electromagnetic interference, or EMI, has also occurred. Systems that are operated electronically might suffer significant disruptions if exposed to microwave radiation on their electronic components. Furthermore, exposure to microwaves may be harmful to a person's health, impairing their immune system, erratic heart rate, and mental state. Therefore, it is imperative to find a functioning material that can absorb electromagnetic (EM) waves and either dissipate or transform the EM energy into

another kind of energy. To reduce microwave reflection and steal highly valuable things, it is necessary to employ materials that absorb microwaves and have broadband absorption. Right now, a microwave-absorbing material needs to be lightweight, have a large effective frequency spectrum, and have significant absorption to meet the high demand of next generation equipment.

Many nanostructured materials with distinct size and shape have been created as sophisticated electromagnetic materials over the past few decades. Morphology undoubtedly has a significant impact on the characteristics of absorption. One-dimensional nanostructures have garnered significant interest among nanomaterial morphologies owing to their unique chemical and physical characteristics, particularly their increased specific surface area and lower size. Rod-like Te tends to have a highly anisotropic growth due to its distinctive helical-chain crystal structure, which results in special features including photoconductivity and optical response in optical electrical devices. Te's many distinct qualities should inspire us to anticipate its microwave absorption capabilities. Furthermore, as far as we are aware, not many studies have been conducted on high-quality Te as novel microwave absorbers that focus on the effect of size and form.

Te 2D Sheet:

It has recently been determined that van der Waals epitaxy (vdWE) is a simple synthesis method in the growth Comprising vertical heterostructures made of layered materials that are ultrathin in two dimensions (2D). In contrast to traditional heteroepitaxy, vdWE makes use of substrates like fluorophopite mica, whose surface lacks surface dangling bonds and is hence chemically inert. Rather than strong chemical bonding, weak van der Waals interaction connects the overlayer and substrate in the vdWE development.8 Therefore, by avoiding the rigorous requirement of lattice matching, vdWE can produce an overlayer that is devoid of defects and has a different crystalline symmetry than the substrate.

Furthermore, overlayer can be properly relaxed in the heterointerface with no undue strain thanks to vdWE.

Due to its exceptional properties, vdWE is a potent process for growing a wide range of 2D layered materials with a high degree of single crystallinity. As was initially stated, vdWE has been effectively used to create atomically thin III–VI semiconductor

flakes on mica, layered topological insulator Bi2X3 (X = Se or Te) nanoplates on h-BN9 or mica, and transition-metal dichalcogenide nanoplates on graphene or mica. In the meanwhile, other scientists have focused their attention on the vdWE development of nonlayered materials, such as GaAs nanowire arrays on graphene, ZnSe quantum dots on GaSe, ZnO nanowire arrays on graphene, and InAs nanowire arrays on graphene. The flexible and translucent fluorophlogopite mica sheets were coated with 2D hexagonal Te nanoplates deposited using vapor phase extraction (vdWE). The resulting 2D hexagonal Te nanoplate exhibits excellent solitary crystalline with thin thickness (30–80 nm) and considerable lateral dimensions (6–10 μm). Te ads have a high rate of migration along the mica surface due to the lack of a surface dangling bond on the mica substrate and so quickly travel in the direction of growth sites, causing the 2D Te hexagonal Te nanoplate to develop laterally quickly without requiring a tight lattice match.

Te Quantum Dots: Quantum dots (QDs) are nanoscale semiconductor particles that possess unique optical and electronic properties due to quantum mechanics. Typically ranging from 2 to 10 nanometers in diameter, quantum dots exhibit quantum confinement effects, which significantly alter their electronic and optical behaviours compared to bulk materials.
Key features of quantum dots are as follows:

1. Quantum Confinement: In quantum dots, there are three spatial dimensions in which the travel of electrons and holes—electron vacancies that behave like positively charged particles—is constrained. Due to this confinement, distinct optical and electrical properties are produced that are akin to those of discrete energy levels found in atoms.

2. Size-Dependent Properties: The size of quantum dots greatly influences both their energy levels and, as a result, their optical characteristics. The blue end of the spectrum is emitted by smaller dots due to their higher energy gaps, whereas the red end of the spectrum is emitted by larger dots due to their lower energy gaps. Because of their tunability, quantum dots' light emission colour may be precisely controlled.

Concerns about the environment and human health are raised by the usage of some toxic elements in quantum dots, such as cadmium. It is still difficult to guarantee the long-term stability and reliable operation of quantum dots in diverse applications. Because of their special qualities, quantum dots provide a wide range of applications and constitute a significant achievement in nanotechnology. The goals of ongoing research are to increase their application in both new and established technologies, decrease their toxicity, and improve their synthesis.

Motivation:

Nanowires could be utilized in the electronics sector to connect minuscule parts into incredibly tiny circuits. Research in the subject of semiconductor nanowires has been spurred by the difficulty of continuously scaling microelectronic devices to satisfy industry targets, such as Moore's Law and the industry's diversification into novel materials for specialized purposes. The fierce rivalry for a piece of the $30,40,00,00,000 (USD) worldwide semiconductor market has fueled the growth of the field of semiconductor nanowires, giving rise to novel materials, inventive production methods, and inventive breakthroughs in the design of semiconductor nanowire devices. Compared to traditional planar materials, nanowire materials have many advantages, such as FET (field-effect transistor) uses. By enabling more effective control overcharge carriers in the FET device's channel, nanowires lessen the impacts of short channels. Increased device density can be accomplished on a given chip by using multigate architectures, like the Generic Authentication Architecture (GAA), which promote the development of shorter channel devices. Furthermore, it has been shown that a variety of materials can be fabricated into nanowires, even if these materials may not be easily made into wafers.

Application:

Nano Generator:

A nanogenerator is a machine that uses materials and structures at the nanoscale to transform mechanical or thermal energy into electrical energy. Utilizing piezoelectric, triboelectric, or pyroelectric effects at the nanoscale is the fundamental idea behind

nanogenerators. This is a thorough rundown of nanogenerators, covering kinds, operation, materials, and applications.

Nanogenerator Types

1.**Piezoelectric Nanogenerators (PENGs):**

Working Principle: PENGs produce electricity by use of the piezoelectric effect, which is the process by which some materials, when subjected to mechanical stress, produce an electric charge.

Materials: PZT (lead zirconate titanate), $BaTiO_3$ (barium titanate), Te nanowires, ZnO nanowires, and PVDF (polyvinylidene fluoride) are examples of common piezoelectric materials.

2. **Triboelectric Nanogenerators (TENGs):**

Working Principle: TENGs produce electricity by use of the triboelectric effect, which is the process by which two distinct materials come into touch with one another and separate, producing electrical charges.

Materials: A variety of polymers are utilized, including polytetrafluoroethylene (PTFE), polydimethylsiloxane (PDMS), and other dielectric materials.

3. **Pyroelectric Nanogenerators:**

Working Principle: The pyroelectric effect, which occurs when some materials produce an electric charge in reaction to a change in temperature, is how these devices generate power from temperature variations.

Substances: Common pyroelectric materials are $BaTiO_3$, PZT, and PVDF.

Working principle

1. Nanoelectric Piezoelectric Generators: A voltage is produced across a piezoelectric material when mechanical stress is applied because it causes polarization and an electric field. Electrical power can be produced by utilizing this-effect.

2. Nanoelectric Triboelectric Generators: Electrons move from one material to the other when two materials with differing electron affinities come into contact and then separate, producing a potential difference. An external circuit can be driven by an alternating current (AC) by repeated contact and separation.

3. Pyroelectric Nanogenerators: Variations in temperature alter the spontaneous polarization of pyroelectric materials, which produces an electric field and voltage as a result.

Application:

1. Harvesting Energy: Wearable Technology In order to capture energy from body movements, nanogenerators can be included into apparel and accessories.
Obtaining energy from wind, river flow, and surrounding vibrations is known as environmental-energy.
2. Medical devices with self-powered sensors: These are sensors that track physiological signals without requiring external power sources.
Environmental Monitoring: Monitoring environmental factors such as temperature, pressure, and pollution levels by placing self-powered sensors in outlying-areas.
3. Micro and Nano Systems: Microelectromechanical systems (MEMS) and nanoelectromechanical systems (NEMS) are powered for a range of applications, such as sensors and actuators.
4. Consumer Electronics: Portable Electronics: Increasing the battery life of smartphones, tablets, and other portable gadgets or offering a backup power source.

Chapter – 2
Instrumentation

In this chapter, mostly apparatus and instruments, which were used while characterization of the samples has been discussed. A brief description about their working principle has also been given.

Morphological Analysis:

The scanning electron microscope (SEM) is a tool used to study and analyze the shape of microstructures. By scanning the surface of a specimen with an electron beam SEM produces various signals that are converted into visual images displayed on a cathode ray tube (CRT). Two methods are commonly used to generate the electron beam; emission, which controls electron emission using energy and field emission. In electron microscopes field emission electron guns (FEG) are preferred over electron guns. The FESEM allows for the observation of small surface features, on partially assembled objects. Biologists, chemists and physicists utilize this technology to explore structures as 1 nanometer in size. With the FESEM researchers can investigate polymers, microchip coatings well as DNA and organelles, within cells.

Sample Preparations:

To examine specimens using the SEM they must be suitable, for vacuum conditions (~ 10 5 mbar) as the SEM functions in such an environment. This means that analyzing liquids or solids containing water or other volatile substances directly is not feasible. To avoid contaminating the SEM specimen chamber fine powder samples should be securely attached to a substrate, on a specimen holder. Non-conductive materials should be coated with a layer of material by spraying or evaporation and then connected to a conductive specimen container. Common coating materials include carbon, gold (Au) platinum (Pt) palladium (Pd) and their alloys.

Components Of FESEM:

Electron Guns:

A stable electron beam from the electron cannon that has a high current, small spot size, adjustable energy, and minimal energy dispersion is required for modern SEM systems. Different types of electron guns are used in SEM systems, and the quality of the electron beam produced by each type varies greatly. Lanthanum

hexaboride (LaB6) or tungsten "hairpin" cathodes were used in the first SEM systems, but field emission sources,

which now provide higher current and lower energy dispersion. The longevity of the emitter is a crucial consideration when selecting electron sources.

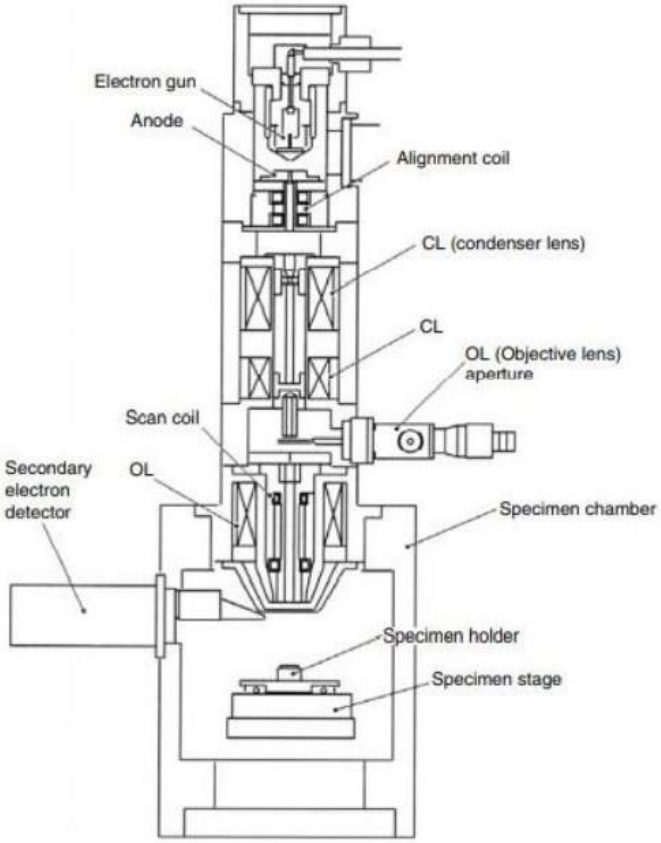


Figure 1: Schematic Diagram of FESEM

Electron Lenses:

Electron beams can be concentrated by magnetic or electrostatic fields. However, the SEM system only employs a magnetic field since an electron beam under magnetic field control has less aberration. Electromagnets can be used to alter the routes taken by electrons.

Condenser Lenses:

The electron beam will diverge after leaving the emission source and going through the anode plate. The electron beam is converged and collimated into a nearly parallel stream by the condenser lens. A copper coil creates a magnetic field that is applied to two pieces of iron pole that are symmetrical in rotation to form a magnetic lens. The electron beam can pass through the hole in the midst of pole pieces.The electron beam is influenced (focused) by the magnetic field via the lens-gap that divides the two pole components. The condenser lens current can be changed to alter the focus point location.

Scan Coils:

The scan coils cause the electron beam to be deflected in a zigzag pattern as it travels over the object. The movement of the scan is timed to coincide with the formation of the image on the screen. The scan velocity controls both the screen refresh rate and the amount of noise in the image. In scan coils, upper and lower coils are frequently employed to stop a circular shadow from forming at low magnification.

The Objective Lens:

It will diverge below the condenser aperture, the electron beam. The electron beam is further demagnified and focussed into a probe point on the specimen surface using objective lenses. The diameter of the electron beam on the specimen surface (spot size) is decreased as Fundamentals of Scanning Electron Microscopy 15 and aperture size, which enhances image resolution.

The Stigmator Coil:

The stigmator coils are employed to make the beam precisely circular by correcting irregularities in the x and y deflection of the beam.
The image seems distorted and stretched when the beam is ellipsoidal as opposed to circular.

Object Camber:

The item is covered with a conductive coating and then set on a designated holder. The object is placed on a moveable stage and brought into the high vacuum

section of the microscope via an exchange chamber. The position of the scintillator, or secondary electron emission detector, in the chamber is behind the object holder.



Figure 2: FESEM (Hitachi S-4800) set up

Image Formation:

Complex interactions take place when an electron beam from a SEM impinges on a specimen surface, stimulating various signals for SEM inspection. It is possible to collect and display specimen current, transmitted electrons, back scattered electrons (BSEs), and secondary electrons on a monitor. The composition of the material is determined by analyzing the excited x-ray or Auger electrons. This part will cover the principle of creating pictures with different signals and the interactions of the electron beam with the specimen surface.

Optical Property Analysis:

UV-VIS near Infrared Spectroscopy:

The ultraviolet-visible spectral region is used in the measurement of optical transmittance, absorbance, and reflectance by a UV-Vis near Infrared (UV-Vis-NIR) spectrophotometer. UV-Vis near Infrared (UV-Vis-NIR) Spectrophotometer: This

instrument measures the optical transmittance, absorbance, and reflectance in the UV-visible spectral region. UV-Vis Absorption Spectroscopy: This type of spectroscopy is used for the determination of the percent of radiation absorbed, transmitted, or reflected at each wavelength. Traditionally, this is done by detecting absorption while moving the wavelength range. The extent of multiple bond or aromatic conjugation in molecules is one of the very practical uses in organic chemistry. More than absorption, the technique can be extended to gases and solids and measure reflected light instead of transmitted light. Light absorption can be described by two fundamental laws as:

Lambert's Law -The proportion of incident light absorbed by a transparent medium is independent of the intensity of the light (provided that there is no other physical or chemical change to the medium). Therefore, successive layers of equal thickness will

$$\frac{I}{I_0} = T$$

transmit an equal proportion of the incident energy. Lambert's Law can be expressed by

where is defined as the intensity of the transmitted light, I_0 is the intensity of the incident light, and is the Transmittance.

Beer's Law-The absorption of light is directly proportional to both the concentration of the absorbing medium and the thickness of the medium in the light path.

A combination of the two laws (known jointly as the Beer-Lambert Law) defines the relationship between (A) and transmittance (T).

$$A = log\frac{I_0}{I} = log\frac{100}{T} = \varepsilon cb$$

Where, A= Absorbance (no unit)

ε = molar absorptivity ($dm^3mol^{-1}cm^{-1}$)

b = Path length (cm) c = molar concentration (mol dm^{-3})

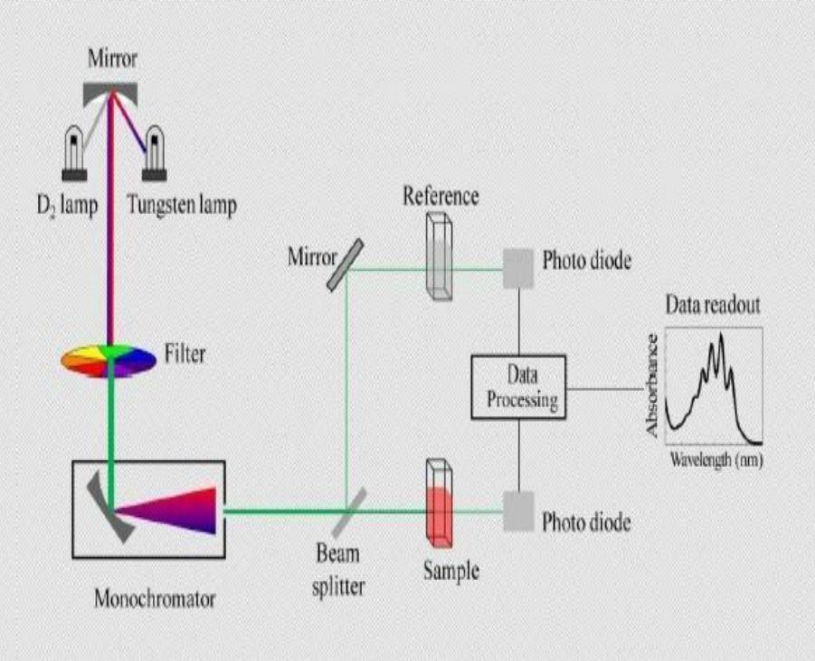


Figure 3: Basic Principles of UV-VIS Spectroscopy

Light reflection and reflectance spectra

The accessory collects the back reflected, diffusely dispersed light-part of which is absorbed by the sample-and directs it to the detector optics. Diffuse reflection is that part of a beam which is dispersed within a sample and which returns to the surface. A spectrometer beam is directed into a sample where it is reflected, dispersed, and transmitted through the material, resulting in diffuse reflectance, shown on the right.

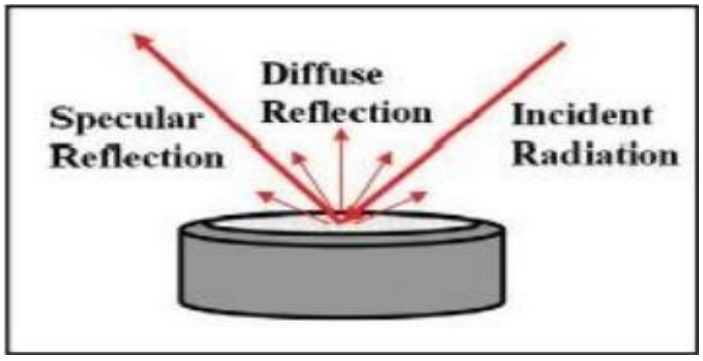


Figure 4: Diffuse and Specular Reflectance

In diffuse reflectance sampling, the other factors that also contribute to good spectral quality are packing, homogeneity, refractive index, and particle size. Despite all these sample preparation processes, the raw diffuse reflectance spectra would look different from its transmission counterpart-stronger than predicted absorption from weak IR bands. One can do a Kubelka-Munk conversion to a diffuse reflectance spectrum in order to adjust for these inconsistencies.

Kubelka-Munk Function

$$F(R) = \frac{(1-R)^2}{R} = \frac{k}{s}$$

The variables R, k, and s represent the absolute reflectance of the sampled layer, the molar absorption coefficient, and the scattering coefficient, respectively. The spectrum above shows the spectral conversion for ibuprofen determined using diffuse reflectance by performing a transmission spectrum data base library search, one can quickly identify the Kubelka-Munk converted spectrum for ibuprofen, which compares favourably to the transmission spectrum.

Components UV-Vis Spectrophotometer:

1. Spectrophotometer consists of the following components.
2. A source of radiation of appropriate wavelengths.
3. Monochromator and optical geometry.
4. filter Sample compartment.
5. Detector, Photomultiplier, Measuring system, computer.



Figure 5: UV-VIS-NIS (SHIMADZU UV-3600) Spectrophotometer

Photoluminescence:

PL spectroscopy is contactless, nondestructive, and comparatively easy. It could be applied to the determination of surface structure, recombination mechanism, band gap, impurity level, defect detection, fluorescence property of materials, and excited states of a material. Photoluminescence is a process whereby a material absorbs photons or EM radiation and reradiates photons.
Quantum mechanically this would be described as an excitation to a higher energy level followed by the emission of a photon that returns the system to the lower energy state. The prefix photo identifies this as one of many types of luminescence, or light emission, characterized by photo excitation, or stimulation by photons. The energy of a photon is the energy emitted when an orbital electron in a molecule, atom, or nanostructure that is excited by light to higher quantum state returns to its ground state.

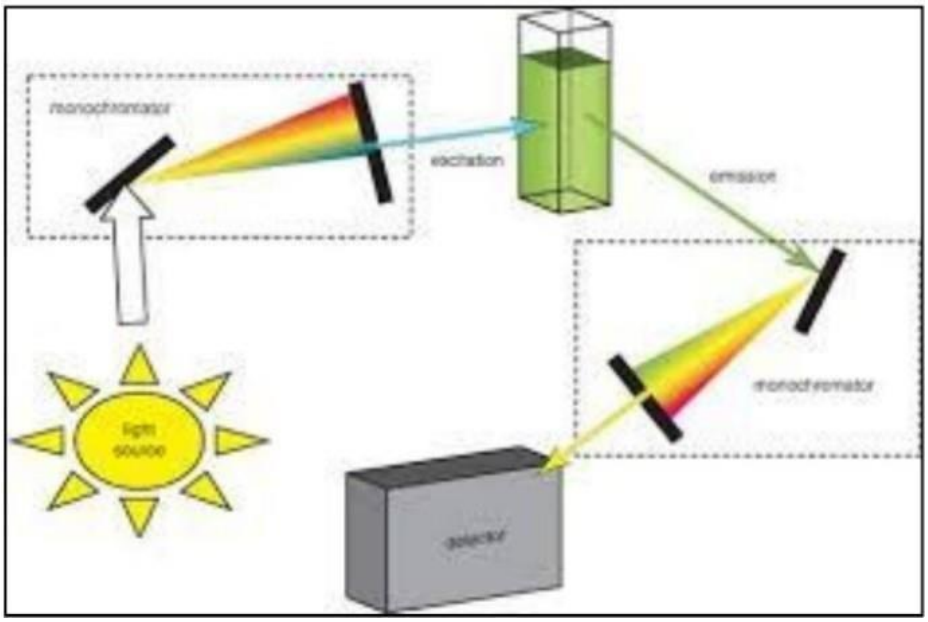


Figure 6: Basic Principle of Photoluminescence

Spectroscopy:

Schematic diagram for photoluminescence In figure, the spectroscopy is shown. Light focussed onto a material, through photo excitation, electrons therein are moved into the available excited states. As the electrons then return to their ground state, the excess energy is released and could or could not emit light-a radiative process-or non-radiative emission. The energy of the emitted light, photoluminescence, is linked to the energetic difference between the two electronic states involved in the transition from excited state to ground state. The relative contribution of the radiative process determines how much light is emitted.
Emitted light has less energy in general due to its longer wavelength than the absorbed radiation.

When the absorbed electromagnetic radiation is strong enough, one electron can absorb two photons. Such a process, two-photon absorption, may lead to the emission of light with a wavelength shorter than the one corresponding to the absorbed energy. If the wavelength of emitted radiation and that of absorbed light is the same, one deals with resonance fluorescence. That is to say, photoluminescence is the process

whereby light is absorbed in the invisible ultraviolet region of the spectrum, and that energy is released as light into the visible spectrum.

By definition, a fluorophore or fluorescent molecule is recognized by its ground state, S0, and its first, electronically, excited state, S1. S1 is a molecule that has many relaxation modes.

It can undergo a process termed "non-radiative relaxation," in which the vibrational and heat energy from the excited state are transferred to the surrounding solvent. Excited organic molecules can also de-excite by way of transition to a triplet state, which in turn can de-excite by secondary nonradiative relaxation processes or phosphorescence. A relaxation of an S1 state can result also from interaction with another molecule through fluorescence quenching. Molecular oxygen (O2) is an extremely effective fluorescence quencher because of a special triplet ground state.The Spectro fluorometer is made up of the following different parts:

(1) Excitation monochromator

(2) Cell holder

(3) Monochromator with emission

(4) Photomultiplier tube on the monitor side

(5) Photomultiplier tube with fluorescence side

Utilizing the Horiba Jobin Yvon Fluromax spectrofluorometer, photoluminescence analysis was performed. This spectrofluorometer's photo is displayed:



Figure 7: Photoluminescence Spectroscope

X-Ray Diffraction (XRD):

X-ray radiation is a form of high energy electromagnetic radiation of very short wavelengths on the order of solid atomic spacing. A fraction of an x-ray beam that impinges on a solid material is scattered in all directions by electrons bound to every atom and ion that is in its path.

Now let's consider the requirements for X-ray diffraction by a periodic array of atoms. Diffraction occurs when a wave interacting with a series of evenly spaced obstacles that are of comparable magnitude to the wavelength and capable of scattering the wave. Besides, diffraction is interference by particular phase relationships that have been set up between two or more waves that have been scattered by the obstacles. The phase relation of the dispersed waves, depending on how large the path length difference is. When its path length is an integral number of wavelengths, one may result.

Bragg's Law

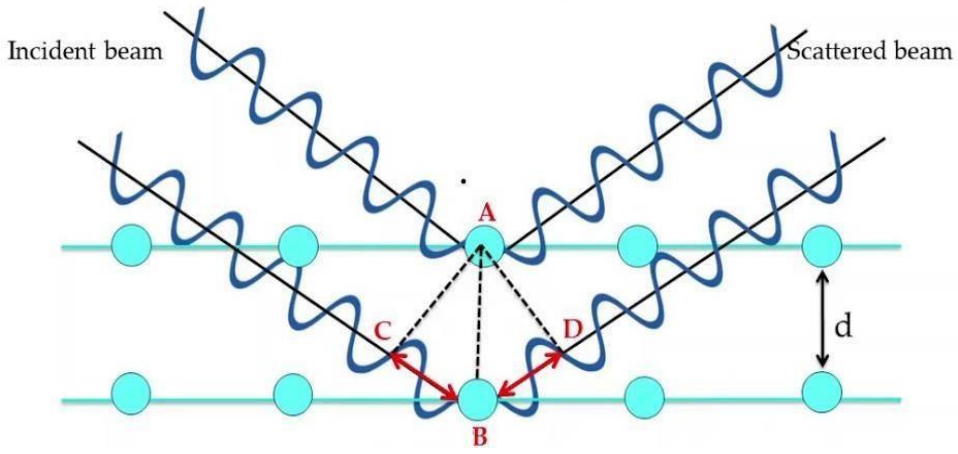


Figure 8: Brag's Law of diffraction

Consider now two parallel atomic planes, separated by the interplanar distance d and having identical h, k and l Miller indices. For this study consider that these two planes are incident with parallel, monochromatic, coherent (in-phase) x-ray beam of wavelength λ at an angle of Θ. Two rays are scattered in this incident beam by atoms A and B. If the path length difference, i.e. CB+BD, between the scattered waves is equal to an integral number, n of wavelengths then constructive interference of the scattered waves also occurs at an angle of σ to the planes. Hence, the condition for diffraction is

$$n\lambda = CB+BD$$

$$\text{or, } n\lambda = d\sin\Theta + d\sin\Theta$$

$$\text{or, } n\lambda = 2d\sin\Theta$$

Production of x-ray:

X-rays are created when a heated filament (typically tungsten) emits an electron beam at a metal target (commonly Cu or Mo). When electrons from the target atom's K-shell (1s) are ionized by the incident beam, vacancies are created that are filled by electrons falling from the L (2p) or M (3p) levels, which releases X-rays. Kα and Kβ lines are the result of this.

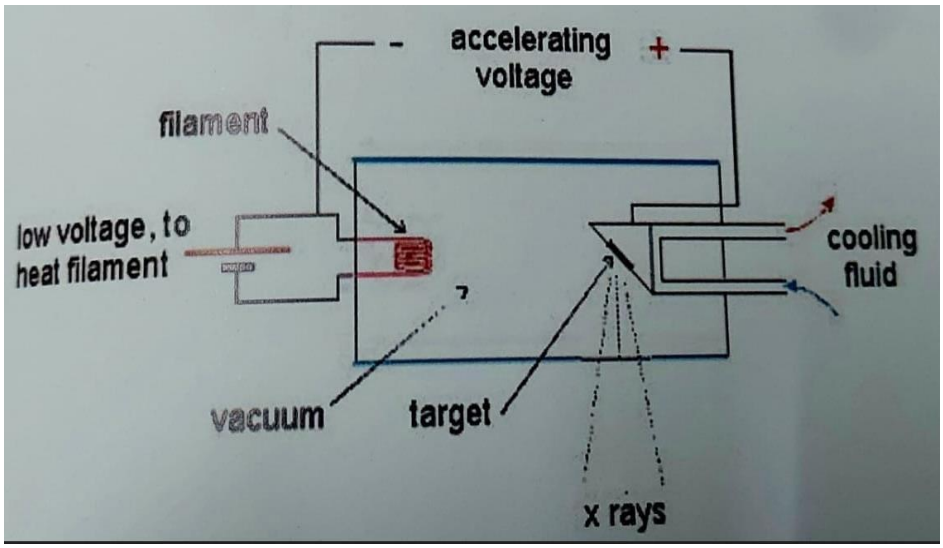


Figure 9: Production of X-rays



Figure 10: X-Ray Diffraction (Bruker D8 advance)

Particle Size determination by Scherrer's formula:

The sample's experimentally determined diffraction patterns are compared to the standard powder diffraction files that the JCPDS has made available. Scherrer's formula was utilized to determine the average grain size of the samples:

$$D = \frac{0.9\lambda}{\beta \cos \theta}$$

where β is the complete breadth at half maximum intensity in radians and λ is the x-ray wavelength.

It is crucial to understand that the particle size has a lower bound given by Scherrer's formula. This is because the diffraction peak broadening has a great number of causes: excluding the dimensions of the particle, the other two most important causes are due to inhomogeneous strain and experimental errors. If all the other causes were zero, the peak width would be determined by Scherrer's formula and depend exclusively upon the particle size. The size of the particle can be larger than that given by this equation, since the other contributors to peak broadening are not necessarily zero: the "additional" peak broadening coming from the extra information.

- **FOURIER TRANSFORM INFRA-RED SPECTROSCOPY (FTIR):**

FTIR spectroscopy can be used to study the vibrational properties of synthesized materials. Besides, the chemical composition and structure, in general, govern the peak position of the absorption and band for the thin film, apart from its shape.
FT-IR spectroscopy is a standout way for performing an infrared spectrum. Infrared spectroscopy detects the infrared radiation's transmission of a sample. The sample partially absorbs the infrared light and partially transmits. The resulting spectrum provides a molecular fingerprint that exhibits the absorption and transmission of the sample's molecule. Just as a fingerprint, no two fingerprints of different molecule configurations have the same infrared spectrum. So, there are tremendous applications in infrared spectroscopy..

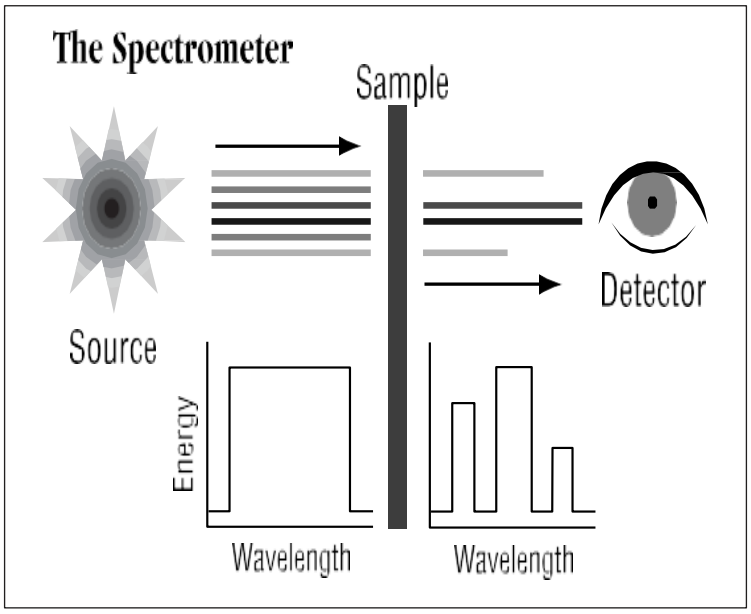


Figure 11: Spectrometer

So, what kind of information can FT-IR give you?

- It can determine the quality or consistency of a sample
- It can determine the number of components in a mixture
- It can identify unknown materials

Why FT-IR?

Fourier Transform Infra-Red (FT-IR) spectrometry was developed to overcome the disadvantages of dispersive instruments. The main issue was the slow scanning process. Instead of measuring one infrared frequency at a time, a means of measuring them all simultaneously had to be devised. To achieve this end an extremely simple optical instrument called an interferometer was used. One signal from the interferometer has all infrared frequencies "encoded." The signal can be measured, in general, in a matter of fractions of a second. As a result, the time element of each sample is reduced from several minutes to only a few seconds. Most interferometers divide the entering infrared beam into two optical beams by means of a beam splitter.



Figure 12: An interferogram signal

One beam is reflected by an installed flat mirror. A mechanism allows the other beam to reflect off a flat mirror that moves just a very small distance away from the beam splitter. The two beams are recombined at the beam splitter when they meet again reflecting off of their own mirrors. These two beams "interfering" with each other, because one beam path is fixed and the other is always changing when its mirror is moving, gives the resulting signal that leaves the interferometer.

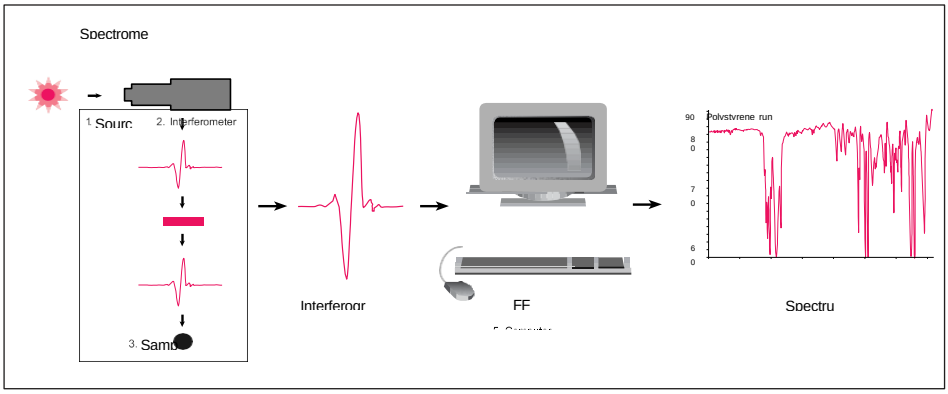


Figure13: Process of generating an FTIR spectra

The resultant signal is called an interferogram, and it has the special ability to contain information on each infrared frequency that originates from the source in each of the signal's data points (which are functions of the moving mirror position). This indicates that when measuring the interferogram, all frequencies are measured at the same time. Measurements are made very quickly because of the interferometer. Because the analyst needs a frequency spectrum—a depiction of the strength at each particular frequency—to make an identification, the observed interferogram signal cannot be directly evaluated. Some method of "decoding" each of the different frequencies must exist. This can be done using a well-known mathematical method called the Fourier transformation. This modification is carried out by the computer and then presents the user with the desired spectral information for analysis.

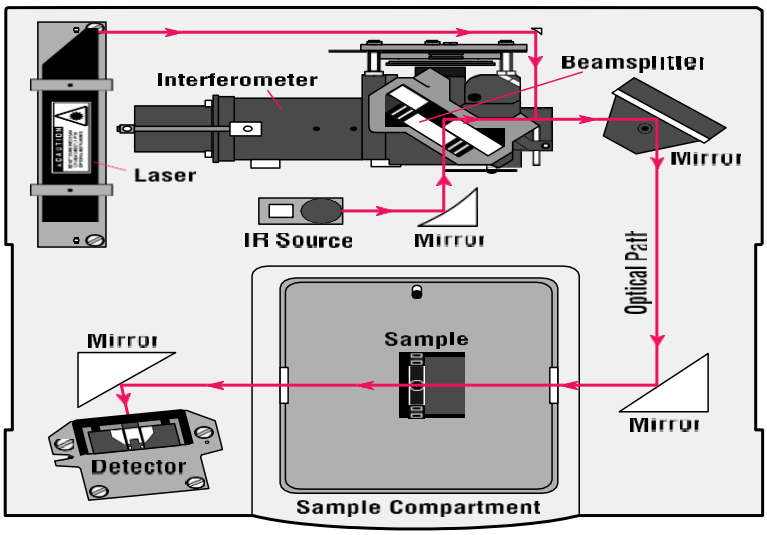


Figure 14: A simple spectrometer layout

THE SAMPLE ANALYSIS PROCESS:

This is how the typical instrumental method works:

1. **The Source**: Infrared radiation comes from a black-body source that glows. The amount of energy that is sent to the sample (and, eventually, the detector) is controlled by the aperture that this beam passes through.
2. **The Interferometer**: The interferometer converts light into a digital format by means of "spectral encoding." The interferometer then outputs the interferogram signal.
3. **The Sample:** The beam enters the sample compartment and is either transmitted through or reflected off the sample's surface, depending on the sort of analysis being done. This is the point of absorption for the energy frequencies particular to the sample.
4. **The Detector**: The beam finally reaches the detector, where it is measured.The detect5, or used were created specifically to measure the interferogram signal.
5. **The Computer:** The Fourier transformation is carried out by the computer after the measured signal has been digitalized and supplied to it. The finished infrared spectrum is then shown to the user for analysis and any additional modification.

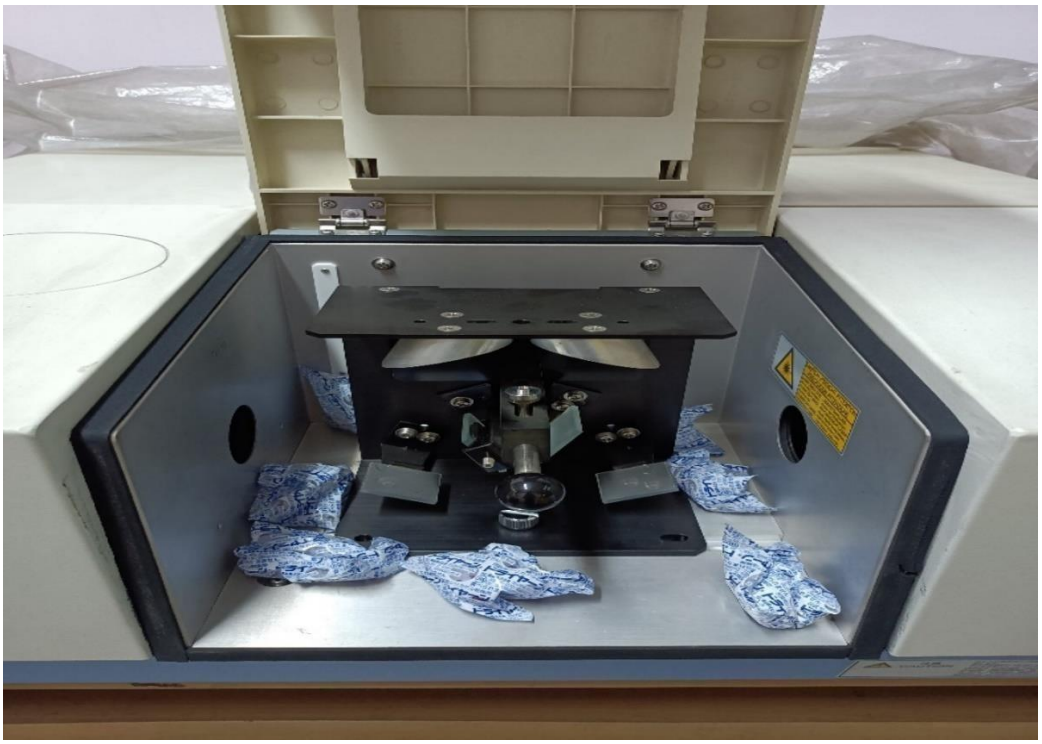


Figure 15: Internal components of FTIR instrument

A background spectrum needs to be assessed as well because the absorption intensity needs to be determined on a relative scale. This measurement is often done without a sample in the beam. This is comparable to the measurement of "percent transmittance" obtained with the sample in the beam. With this technique, a spectrum free of any instrumental features is produced. Consequently, all observed spectrum features are entirely sample-dependent. A single background measurement can be used for many sample measurements because of the distinctive spectrum of the device.

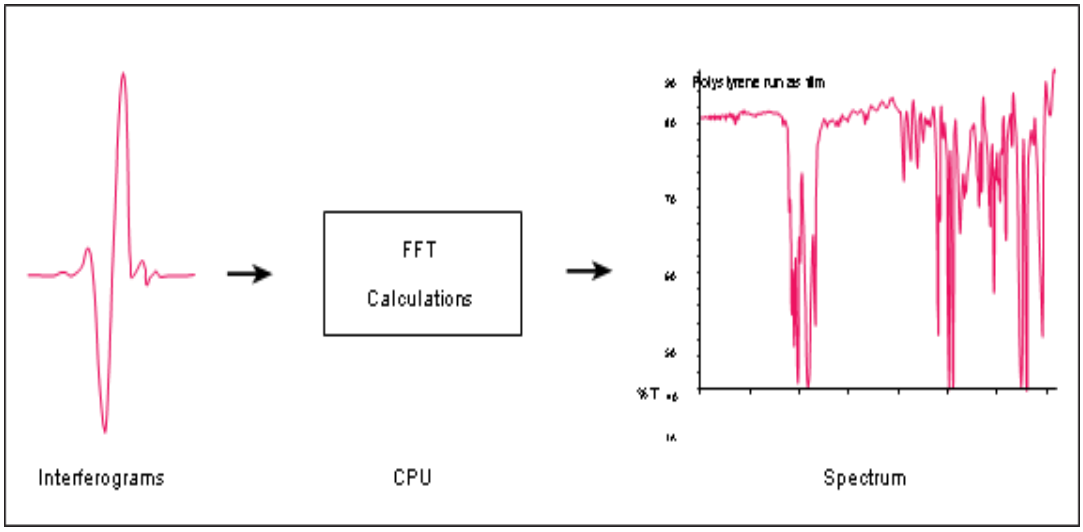


Figure 16: Internal Process for the formation of FTIR spectra

- **Raman Spectroscopy:**

Raman scattering was first observed by Dr. C.V. Raman in 1928 and was used to investigate the vibrational states of many molecules.

- **Raman System:**

The constituents that make a standard Raman system include: (1) excitation source, usually a laser; (2) optics for sample illumination; (3) double or triple monochromator; and (4) signal processing system with an output device, amplifier, and detector. A lens serves to focus laser light onto a sample mounted on the sample chamber. An extra lens is used to collect the diffracted light and then focus it at the entrance slit of the monochromator. This acts as a dispersion element for the incoming radiation and effectively rejects stray light. Light collected at the exit slit of the monochromator focuses on the surface of a detector. Inside the detector, this optical signal is converted to an electrical signal, which is further processed by detector electronics. This kind of signal is stored in the computer memory for every predefined

frequency period. In a conventional Raman system that has a PMT detector, which measures light intensity at different frequencies, a monochromator is scanned. A plot of signal intensity against wavenumber shows its Raman spectrum.

- **Principle:**

The process of most of the radiation being scattered by a sample at the same wavelength as the incoming laser radiation when it is exposed to an intense monochromatic light source typically a laser is called Rayleigh scattering. But a tiny percentage of the incoming light roughly one photon per million—is dispersed at a wavelength that differs from the laser's initial wavelength.

1. The sample is excited by laser light.
2. There is a scattering of this light everywhere.
3. A portion of this dispersed light is focused on the detector to capture the Raman spectrum.
4. This spectrum displays light at the original laser (Rayleigh) frequency as well as sample-specific Raman spectrum characteristics.

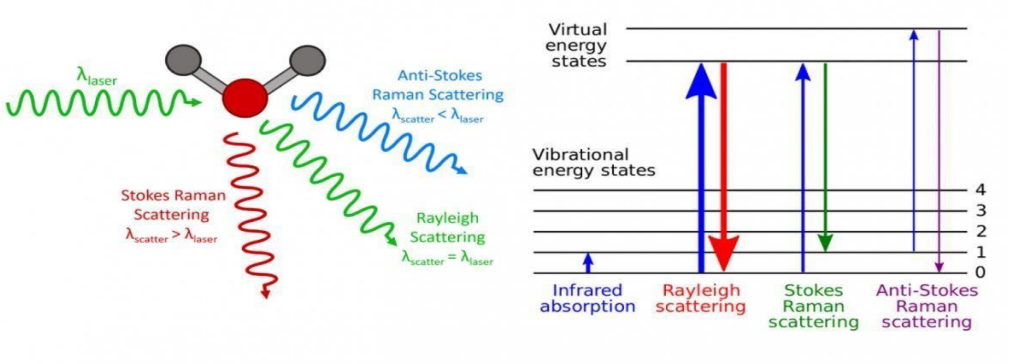


Figure 17: Different types of Scattering

This same transition can be responsible for Raman scattering in infrared absorption between molecular vibration states (M) and (M*). One of the main differences between the Raman and infrared processes is that in the former the photons are either unabsorbed, or but underwent a frequency shift of the same magnitude as the energy of the particular vibrational transition. Parallel to emission, the anti-Stokes process shifts the scattered photons to higher frequencies as they pick up the energy released by the molecules during transitions to the ground state. In the parallel absorption-the

Stokes process-the scattered photons are shifted to lower frequencies as the molecules abstract energy from the exciting photons. The virtual state relaxes in an extremely short time, mostly back to the original ground state. This mechanism leads to the so-called Rayleigh scattering, or scattered light with the same wavelength as the excitation laser. Upon relaxation to the first stimulated level, there is a shift in the Stokes-Raman vibrational level. As compared to laser light, the dispersed light with Stokes-Raman shift is of longer wavelength and lower energy. In the majority of systems, a small portion of molecules start out in an excited vibrational state. A larger energy (shorter wavelength) can be scattered out than that of the original laser light when the Raman scattering process starts from an excited vibrational level and relaxes to the ground state. This type of scattering is named anti-Stokes-Raman scattering. The Raman spectrum of two molecules can be exactly the same, whereby the material amount present determines how much light is scattered and how intense it becomes. Regarding this, the Raman spectrum has provided the sample with qualitative and quantitative information. The Raman spectra were obtained using WITEC alpha 300R-RAMAN spectroscopy.

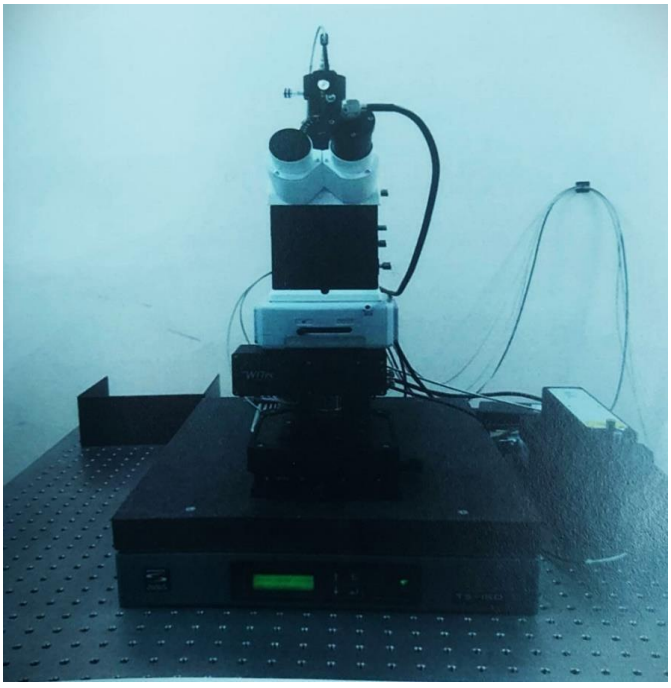


Figure 18: WITEC alpha 300R-RAMAN spectroscopy.

LCR Meter:

Dielectric measurements reveal the electrical properties of insulating materials. A great deal about the permittivity, dielectric loss, and conductivity of the material under test can be learned from these tests. The usual procedure comprises proper test fixtures and an instrument for dielectric measurement, including an LCR meter or impedance analyzer. The following is a step-by-step tutorial on how to perform dielectric measurements:

1.Preparation:

Choose the Material: Decide which insulating material will be examined. **Sample Setting Up**: Cut the sample in accordance with the test fixture specifications to the appropriate size and form. Make sure there are no impurities or dirt on the sample surface.

Adjust the Devices: To guarantee accurate readings, calibrate the measurement system, performing load, short, and open calibrations.

2. Setup:

Assemble the Test Fixture: Put together the test fixture that is suitable for the measurement. Depending on the frequency range and material, common types include coaxial fittings, waveguides, and parallel plate capacitors. **Sample Mounting**: Firmly insert the sample into the test fixture. Make sure the sample and electrodes make adequate contact to prevent air gaps that could skew the measurement.

3. Measurement

Connect to Measurement Device: Using the proper wires, attach the test fixture to the LCR meter or impedance analyzer.

Choose Measurement Parameters: Choose the parameters for the measurement, including the voltage level, frequency range, and measurement sites.

Frequency Range: Select the range to be measured for the dielectric characteristics.

The resulting current is used to determine the dielectric properties. This can vary from a few Hz to Several Hz.

Level of Voltage: Determine the AC voltage that will be applied to the sample. Usually, this falls between a few millivolts and volts.

-**Execute the measurement**: Initiate the process of measuring. To determine the dielectric characteristics of the sample, the device will apply an AC signal and measure the current that results.

4.**Information-Gathering-and-Evaluation**

Data Acquisition: Gather the measurement data, usually consisting of the sample's complex impedance or admittance.

Data processing: Transform the raw data into dielectric parameters, such as loss tangent (tan δ), permittivity (ε'), and dielectric loss (ε'').

The real portion of the dielectric constant, or permittivity (ε'), represents the material's capacity to hold electrical energy.

Loss Tangent (tan δ): A measure of the permittivity to dielectric loss ratio that expresses how effective an insulator a material is.

5.The-Measurement:

Check the Data: Verify the quality and consistency of the measured data. If more measurements are required to verify the results, do so.

Analyse the findings: Determine the material's dielectric characteristics and, if relevant, how they depend on temperature and frequency by analyzing the data.

Document Results: Keep a formal report that contains all pertinent information, such as measurement circumstances, sample specifics, and outcomes.

These procedures will let you measure insulating materials' dielectric characteristics p recisely, which is necessary for using them in a variety of electrical and electronic dev ices.

❖ Literature Review:

From the literature review we have found that in the above table from all the synthesis process the prominent one is one pot hydrothermal synthesis. It is the very easy process and it gives us best form of Tellurene.

From the literature review we also get to know that why we choose tellurene for CV experiment in H_2O_2 sensing.

The reason for using tellurene in the experiments of cyclic voltammetry in hydrogen peroxide sensing is due to its extraordinary combination of properties, hence highly suitable for this type of electrochemical sensing application.
Tellurene, being a 2-D material, has a high surface area-to-volume ratio, hence providing more active sites for the electrochemical reaction. High surface area enhances the sensitivity of tellurine-based sensors to H_2O_2 since more H_2O_2 molecules can effectively adsorb and interact with the electrode surface.

Tellurene possesses good electrical conductivity, which is desirable for efficient electron transfer to take place during the course of redox reactions in cyclic voltammetry. The property means that an electrode based on tellurene will have the efficacy to facilitate the processes of oxidation and reduction of H_2O_2 effectively; hence, it yields clear and distinct electrochemical signals.
Furthermore, it was shown that tellurene exhibits intrinsic catalytic activity, especially for the reduction of H_2O_2. This catalytic property is what tells tellurene to reduce the activation energy of the electrochemical reaction and, therefore, enhances the kinetics of the redox process and thus enables sensors to be more responsive and sensitive to H_2O_2.

Tellurene possesses direction-dependent features due to its anisotropic nature, which can help adjust the sensor's electrochemical performance. By using this anisotropy, the sensor's response to $H2O_3$ may be optimized, perhaps leading to more sensitive and selective detection. Tellurene is a chemically stable substance that works well in a variety of conditions, including the presence of H2O2. For accurate and repeatable sensing findings, the material must be able to sustain its performance across several cycles of the cyclic voltammetry experiment without suffering appreciable deterioration.It is simple to functionalize the surface of ellurene with different compounds or nanoparticles to increase its sensitivity and selectivity towards $H2O_2$. For instance, adding specific binding agents or catalysts to the tellurene surface can enhance

its capacity to detect H2O2 even at low concentrations. Tellurene's bandgap and electronic properties may be adjusted by changing its thickness or putting it under external strain. Because of its tunability, scientists may tailor the substance to certain electrochemical sensing uses, such as the detection of H2O2. The current response in cyclic voltammetry is a crucial indicator of the analyte's concentration. Because of tellurene's high conductivity and catalytic qualities, the cyclic voltammetry experiment produces a strong and distinct signal response that facilitates the detection and measurement of $H2O_2$.

From the literature review we have found that in the table from all the synthesis process the prominent one is one pot hydrothermal synthesis. It is the very easy process and it gives us best form of Tellurene.

Synthesis Method	Morphology	Electrical property	Optical property	Ref
tellurium nanosheets were synthesized through a one-pot hydrothermal reaction. Sodium tellurite (Na2TeO3) powder, polyvinylpyrrolidone (PVP, K-30, Mw = 40000), ammonium hydroxide solution (NH3·H2O), and hydrazine monohydrate (N2H4·H2O) are of analytical grade and have not been further purified. The Te nanosheet synthesis was performed as follows: PVP (1.5 g) and Na2TeO3 (0.046 g) were added to double-distilled	Nanosheet		the 2D Te nanosheets showed excellent optical response under light at wavelengths of 350, 365, 380, and 400 nm.	(8)

water (16 mL) in a 50 mL beaker to form a homogeneous solution by magnetic stirring at room temperature. Then, the NH3·H2O (1.66 mL) and N2H4·H2O (0.838 mL) were successively dissolved in the above solution. Afterwards, the solution was transferred to a 25 mL stainless steel autoclave lined with tetrafluoroethylene and placed in an oven. The reaction was carried out at 180° C with different reaction times from 1 h to 4 h. Then, the autoclave was naturally cooled to room temperature, and the precipitate obtained was washed with deionized water and alcohol by centrifugation at 4000 rpm for 5 min. After that, a silver-gray sample was obtained and then dried at 60° C for at least 12 h. Finally, the precipitate was ground using a mortar and pestle to obtain a fine powder.				

Liquid-phase exfoliation (LPE) is a simple technology for preparing 2D nanosheets. nanosheets can be stripped from large layered materials by high-speed mixing and stirring (e.g., ultrasonication). At present, graphene,76 high-quality low-layer antimonene nanosheets,77 and excellent water-soluble phosphorene 34 have been prepared successively by LPE. Liu et al.78 obtained large-area 2D tellurene nanosheets in ethanol solvent after ultrasonication and centrifugation. It prepared 2D layered Te nanostructures with a width of 41.5–177.5 nm and a thickness of 5.1–6.4 nm by LPE. In addition, which inspires the application of tumor phototherapy in organisms. The use of 2D Te nanosheets prepared by LPE for PDT is reflected in the work. who sonicated raw Te powder in a	Nanosheet		the 2D Te nanosheets showed excellent optical response under light at wavelengths of 350, 365, 380, and 400 nm, which inspires the application of tumor phototherapy in organisms. Te nanomaterials have a good light absorption effect and high photothermal conversion performance under NIR, which is undoubtedly very attractive in the application of PTT	(9)

dimethylformamide bath to break the bonds of large-size Te layers, and a peeled tellurene nanosheet was obtained. Compared with the strict requirements of PVD, LPE has the advantages of low cost, simple operation, and low environmental impact,80 Manna et al.79 used a water–NMP mixed solvent system to significantly increase the stripping yield and stabilize the synthesized nanosheets over a long time.				
A certain amount of Na2TeO3 and HCl was dissolved into a mixture of 25 ml of ethanol and 25 ml of distilled water to give a solution containing 25 mM of Na2TeO3 and 1 M of HCl. Subsequently, 0.5 ml of hydrazine monohydrate (85%) was added into this solution. Then the resulting solution was transferred into a Teflon-lined autoclave of 60 ml capacity. The autoclave was maintained at 100 C	Nano rod			(10)

for 12 h and then cooled to room temperature naturally. The resulting solid products were filtered and washed, and finally dried in a vacuum at 60 C for 4 h				
For a large-scale synthesis of 2D Te used a low temp, substrate- less solution process to fabricate large-area, high quality 2D tellurene. It grew into 2D flakes with edge lengths of 50-100 µm and thickness of 10 to 100 nm by reducing Na2Teo3 in an alkaline solution by hydrazine hydrate (N2H4.H2O) at a temp of 160-200c in the presence of the crystalline surface blocking ligand PVP. Further studied the growth pathway of Te nanoribbons.	Nanorods & Nanowire	(1D) nanowires exhibit excellent electrical properties and ultra-high hole mobility (more than 600 cm2 $V^{-1}s^{-1}$) as typical p-type semiconductors, making them very suitable for the construction of electronic and optoelectronic devices. The bandgap of tellurium is thickness dependent, which allows the bandgap from 0.31 eV to 1.26 eV, making 2D	a typical p-type semiconductor, exhibits a bandgap of 0.35 eV at room temperature, When the size is processed to the nanometres level, it exhibits many unique physical properties, such as high thermoelectric, piezoelectric characteristics, photoconductivity, and nonlinear optical response	(11)

		Te a popular material for constructing photodetectors for broadband detection		
One pot hydrothermal Synthesis	Nano rod	2-D materials have demonstrated singular nonlinear optical properties. In particular, the transition metal chalcogenides (TMDC) exhibit very strong second harmonic generation, but only for few-layer thicknesses were the inversion symmetry of the crystal structure is broken.	To achieving excellent performance with tellurene-based mid-IR modulators, the design can also utilize new semiconductor Electro-Optical materials for optical modulation and switching over diverse spectral bands.	(12)

4.4 mmol of PVP was fully dissolved in 50 mL deionized water. PVP of different molecular weights (M.W. 58,000 or 360,000 g/mol) were incorporated, following the addition of 0.45 mmol of sodium tellurite (Na_2TeO_3, Sigma Aldrich, 99%) to the solution. As the components fully dissolved, the solution became transparent. Hydrazine (N_2H_4, Sigma Aldrich, 98%) and ammonium hydroxide solution (NH_4OH, 28% NH_3, Sigma Aldrich) were added as the reducing agent and pH adjustment, respectively. The dissolved solution was maintained for 10 min. The resulting solution was transferred to a Teflon-lined autoclave and heated at 180 ◦C for 30 h. After the reaction was completed, the Teflon-lined autoclave was left to	Nano wire		Te nanomaterials have a good light absorption effect and high photothermal conversion performance under NIR, which is undoubtedly very attractive in the application of PTT	(13)

cool down to room temperature. The obtained tellurene solution was washed four times with deionized water by centrifugation, and then the cleaned solution was dispersed in ethyl alcohol.				
DFT method		γ-phase is the most stable in the monolayer configuration, while α-phase is more stable when the number of layers is greater than 1. The calculation of the electronic properties necessarely requires the inclusion of SOC corrections. Overall, the bandgap appears to decrease with increasing number of layers for all the studied phases.	Tellurene's thermal conductivity is relatively low compared to other 2D materials like graphene. This low thermal conductivity is advantageous for thermoelectric applications, where maintaining a temperature gradient is crucial for device efficiency.	(14)

Chemical vapor deposition (CVD) is a bottom-up approach where tellurium is vaporized and then condensed on a substrate to form tellurene layers. CVD allows for better control over layer thickness and size, making it suitable for the mass production of high-quality tellurene films. However, this method requires precise control over temperature, pressure, and precursor materials.	Nanowire	ellurene has a direct bandgap, which ranges from 0.35 eV to 1.0 eV, depending on its thickness and strain. This is in contrast to graphene, which has no bandgap, making tellurene particularly interesting for semiconductor applications. The bandgap tunability of tellurene makes it suitable for various electronic and optoelectronic applications, including field-effect transistors (FETs) and photodetectors.		(15)

Mechanical exfoliation is one of the simplest methods to obtain tellurene. It involves physically separating tellurene layers from bulk tellurium crystals using adhesive tapes. While this method is straightforward and produces high-quality monolayers, it is not scalable for industrial applications.	nanosheet	Tellurene exhibits excellent flexibility and mechanical strength. It can sustain significant strain, which can be used to tune its electronic properties. The material's flexibility makes it a candidate for flexible electronics and wearable devices.	Tellurene shows strong anisotropy in its optical properties, which can be exploited in polarization-sensitive photodetectors and other optical devices. It also exhibits high absorbance in the visible and infrared regions, making it suitable for photovoltaic and photodetection applications.	(16)

Chapter 3

Experiments: Synthesis of Samples

Synthesis of Tellurene Material (TE)

e's chain structure makes it simple to synthesize in its 2D form. Te has the ability to generate helical atomic chain nanowires and has a current density higher than other semiconductor nanowires. having a high aspect ratio, such as nanowires, nanorods, and nanotubes, are thought to have a 2D nanostructure59. The structure of the nanowire is easily modifiable and stable. The enhanced loading efficiency of nanotubes is attributed to their hollow internal structure. The techniques for creating 2D Te nanoparticles have been studied and applied extensively. The synthesis of 2D Te nanostructures has been achieved in a number of works to date, mostly using solution reaction synthesis and solid-phase deposition.

Solid-phase synthesis has been reported in many works. The fine structure of Te nanorods was methodically investigated in order to achieve the controlled development of 2D Te nanorods. Ordered 2D Te nanostructures were created using a hydrothermal procedure, and further opportunities for novel applications were suggested. High purity can still be challenging to attain since contaminants are simple to combine with during the solid-phase deposition process. Solution synthesis offers a superior concept as a result.

Large-scale synthesis is guaranteed by the cheap cost of solution synthesis and the generally mild reaction conditions. It was possible to create nanoneedles, nanotubes, and nanorods with controlled lengths and controllable, uniform surfaces using these nanorods, which had an average length of 1.80 ± 0.16 μm and a width of 98 ± 3 nm. It is important to remember that telluric acid has to break down into tellurium dioxide below 150 °C in order for tellurium dioxide to not immediately convert to Te nanorods at excessive temperatures. Moreover, the obtained samples were not physically degraded. Based on the aforementioned study, a solid basis for the ensuing uses of 2D Te nanostructures is also laid by the comparatively extensive research on them.

All reagents used in the experiments were analytically pure without further purification and purchased from Sinopharm Chemical Reagent Co., Ltd. (Shanghai, China). From the literature review we invent that above all the synthesis process, One-pot hydrothermal synthesis is one of the best processes to get the material Tellurene (Te).

- **Materials**

  Cetyltrimethylammonium Bromide (CTAB), Sodium Tellurite (Na_2TeO_3), Minium Assay (oxidimetric) 98%), Ammonium Hydroxide ($NH_3.H_2O$), Hydrazine Hydrate ($N_2H4.H_2O$)

- **Sample Preparation**

  1. First 1.66 ml of Ammonium Hydroxide, 0.75 gm of Cetyltrimethylammonium Bromide and 30 ml of Di-ionised Water (DI) is taken in a 50ml beaker and the beaker is placed in the sonicate for 10 min in room temperature.
  2. Another 0.046 gm of Sodium Tellurite, 0.838 ml of Hydrazine Hydrate and 30 ml of Di-ionised Water (DI) is taken in a 50 ml beaker and the beaker is placed in the sonicate for 10 min in room temperature.
  3. After that both the solution mixed in another 100 ml beaker and placed in the sonicate for 5 min in room temperature.
  4. As prepared solution was then kept in a Teflon auto-clave and packed tightly into hydrothermal metal jacket. Finally, the solution was kept in oven at 180^0 C for 1h, 2h, 3h and 4h for different variation and comparative study of reduced of Tellurene.
  5. After completion of the reactions, the solution was kept for getting settled and cool down to room temperature.
  6. Then, the solution was filtered through adding Ethanol, it helps to remove the polymer and the process is continued for many times.
  7. After that the solution kept in the petri dish for overnight at 50^0 C.
  8. Finally, we get the powder form of Te.

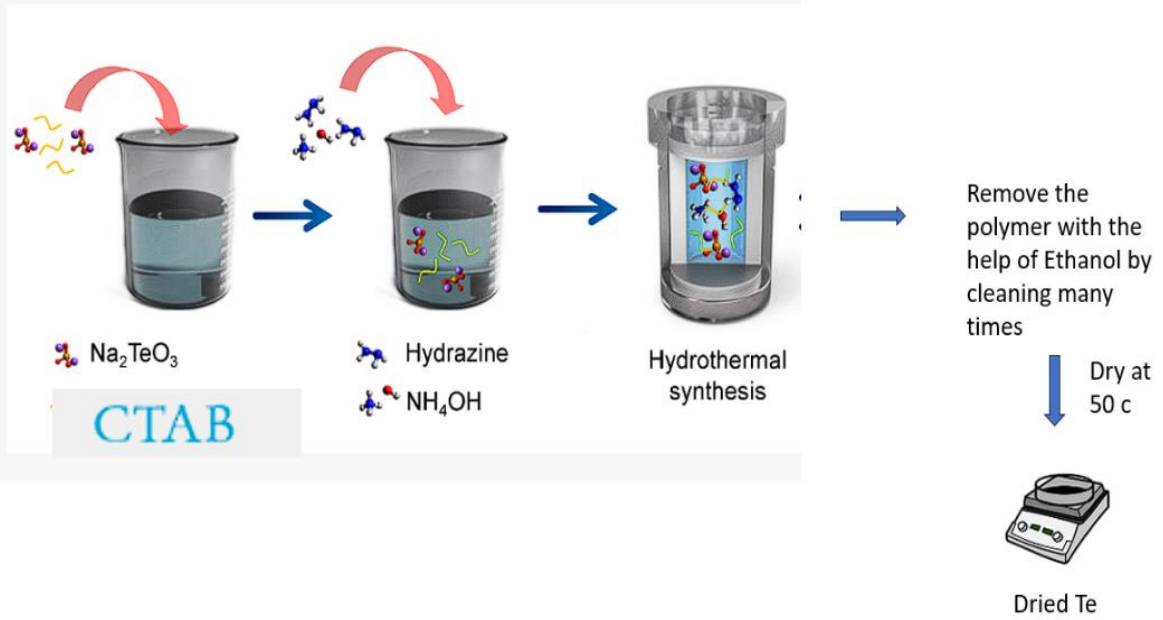


Fig – A simple flow diagram explaining the entire synthesis process.

Chapter 4

Results and Discussion

Crystallographic Characterization & Analysis:

It is crucial to perform X-Ray Diffraction (XRD) on the samples in order to determine their crystallographic nature, including crystal structure, lattice structure, and interplanar spacing, phase and other properties of the sample. XRD analysis of hydrothermally produced Tellurene was done for this study. Here, an XRD analysis comparison and illustrative research for Te 1hr, Te 2hr, Te 3hr, Te 4hr has been conducted and discussed.

- **X-Ray Diffraction Analysis (XRD):**

The XRD tool based its analysis on the diffraction generated by Bragg's law. This law is capable of giving information about the crystal type that the material being used is, if it is in crystallous or amorphous form, and also the distance between a couple of its layers. First of all, with the help of the JCPDS database, every sample's peak XRD plot was matched in order to find out if the substance synthesized in this experiment was indeed reduced Tellurium oxide. The average peak angle 2 theta is comparable to the record from the JCPDS database to confirm that the product is Te exclusively. The hump or broadness of the peak in the graph below confirms that the materials are crystalline in nature.

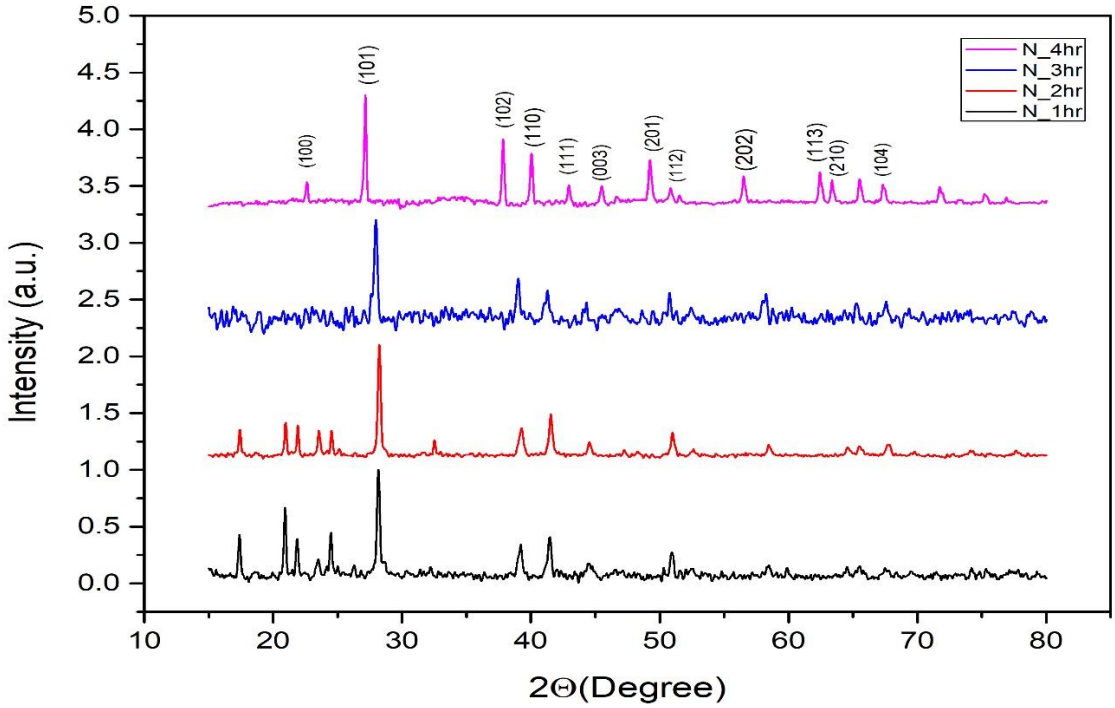


Figure 19: XRD Analysis of N_1hr, N_2hr, N_3hr, and N_4hr

In this graph:

- The x-axis represents the 2θ angle (2 Theta) in degrees, which is the angle between the incident and scattered X-ray beams.
- The y-axis represents the intensity (a.u., arbitrary units) of the diffracted X-rays, indicating the number of X-rays detected at each angle.
- There are four different data sets, each corresponding to a different sample or condition, labeled as N_1hr, N_2hr, N_3hr, and N_4hr. These labels likely represent different processing times (1 hour, 2 hours, 3 hours, and 4 hours).

Key observations:

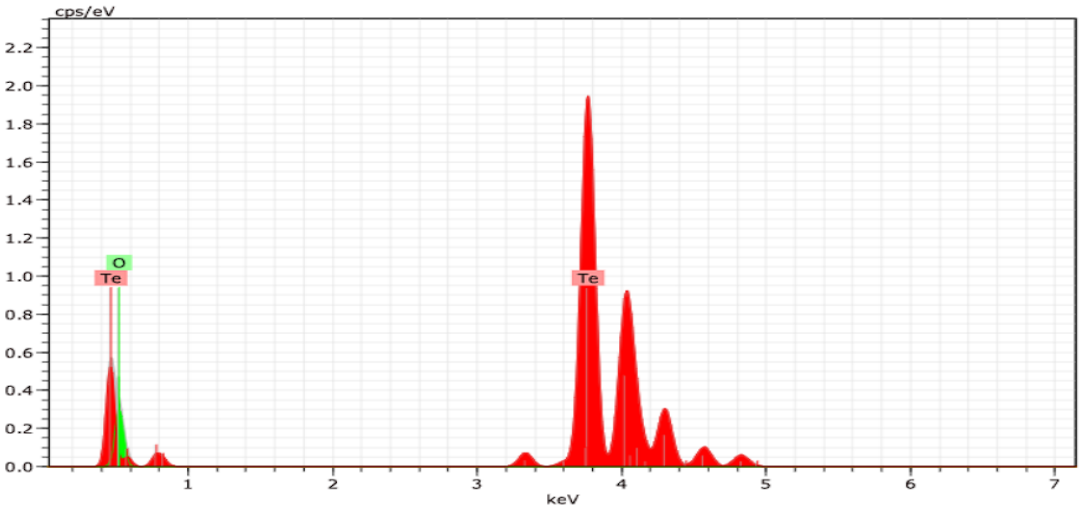
1. Peak Positions: The positions of the peaks along the 2θ axis indicate the presence of specific crystalline planes within the material.

2. Peak Intensities: The intensities of the peaks show the relative amount of each crystallographic plane present in the sample.
3. Sample Differences: Each data set has distinct peaks, indicating differences in the crystalline structure or phase composition due to the different treatment times.

The graph is likely comparing how the crystalline structure of the sample changes with different treatment durations (1 hour, 2 hours, 3 hours, and 4 hours). Differences in peak intensity and position can be analyzed to understand these changes.

- N_1hr (black line): Shows the initial crystallographic structure with a certain set of peaks.
- N_2hr (red line): After 2 hours of treatment, the peak intensities and positions may change, indicating a change in structure or phase.
- N_3hr (blue line): Further changes are observed after 3 hours.
- N_4hr (magenta line): After 4 hours, additional changes in the diffraction pattern are visible.

This XRD analysis is useful for determining how the sample's crystalline structure evolves with time, which can be critical for understanding material properties and optimizing processing conditions.



This graph proves that there is minimal amount of oxygen present and maximum amount of Te. So, it proves that we are going in correct direction and the synthesis process is going towards to make Te crystal.

Element	unn. C[wt.%]	norm. C [wt.%]	Atom. C [wt.%]	Compound norm. Comp. C Error (3 Sigma) [wt.%]	Error (3 Sigma) [wt.%]
Tellurium	106.17	98.74	90.75	98.74	11.76
Oxygen	1.36	1.26	9.25	1.26	1.36
Carbon	0	0	0	0	0

Fourier-transform infrared spectroscopy:

This image shows an FTIR (Fourier Transform Infrared Spectroscopy) spectrum displaying transmittance as a function of wavenumber for a sample measured at different time intervals (1 hour, 2 hours, 3 hours, and 4 hours).

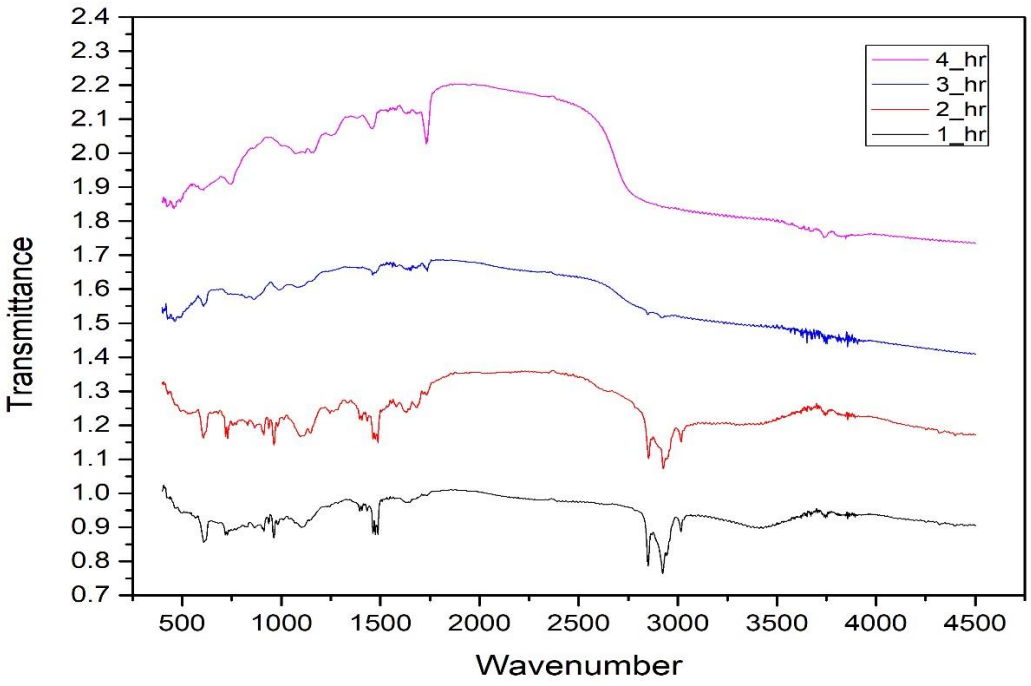


Figure20: FTIR Analysis of N_1hr, N_2hr, N_3hr, and N_4hr

Transmission values throughout the most part of the wavenumber range generally increase with the increase in time from one to four hours. It would be inferred that it is changing either in composition or structure over a period of time in the sample. Notice that this graph provides data on every 1, 2, 3, and 4 hours interval. This therefore serves to demonstrate that, with the increase in time, some sort of chemical or structural alteration takes place within the tellurium-containing material. A possible example could be a case whereby the oxidation of tellurium results in the formation of new Te-O bonds, observable either from the development of new peaks or even the shifting in peaks already existing in the FTIR spectrum.

Broad O-H/N-H Stretch (about 3200–3500 cm^{-1}): The existence of O–H or N–H groups is indicated by the absorption in this region, which gradually loses intensity. **C-H Stretching (about 2800-3000 cm^{-1})**: The vibrations associated with C-H stretching correlate to the maxima in this area. **Carbonyl Group (around 1700 cm^{-1}):** The presence of carbonyl (C=O) groups is indicated by a prominent peak in this area.

Fingerprint Region (below 1500 cm^{-1}): This area has a complex collection of peaks that are specific to the molecular structure of the sample.

Here is a discernible pattern of rising transmittance over the course of the four hours, which could point to a drop in the concentration of absorbing species, potential sample degradation, or a slow-moving chemical process.

Raman Spectroscopy:

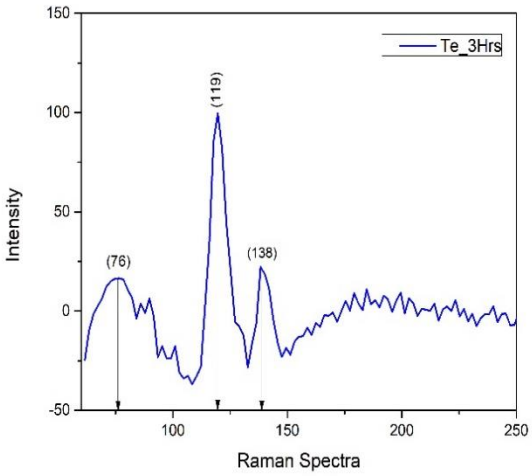


Figure 21: 3_hrs

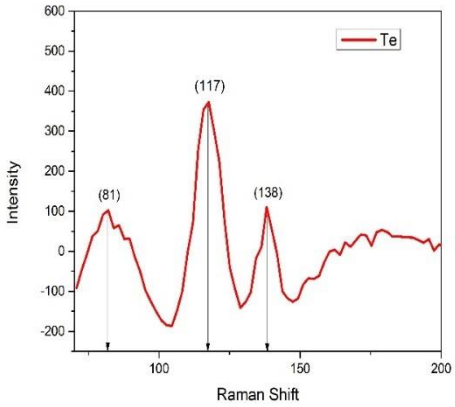


Figure 22: 4_hrs

The provided images depict Raman spectra for tellurium (Te) under two different TIME conditions: "Te_3HRS" and "Te_4HRS".

After these three hours of processing, a number of chemical or structural changes may have taken place on this Te sample, judged by the peak position shifts and intensity changes; changes that could be due to phase transitions, bonding modifications, or even the formation of new compounds or structure.
These shifts could also indicate changes in the crystallinity or degree of disorder of the sample. Increased disorder or alternative crystallographic phases can produce peak

shifting and variations in intensity.
The peak positions match with some of the other journals, which indeed shows that we are going into the right direction. This again leads to the suggestion of the synthesized material being Tellurene.
The Raman spectra recorded significant changes in the course of the Te sample. The shifts in peak positions and changes in peak intensities suggest alterations in the chemical or structural properties of the sample.

PL Spectrum:

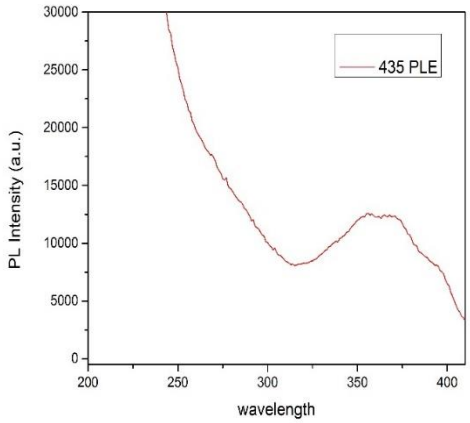


Figure 23: PLE_435

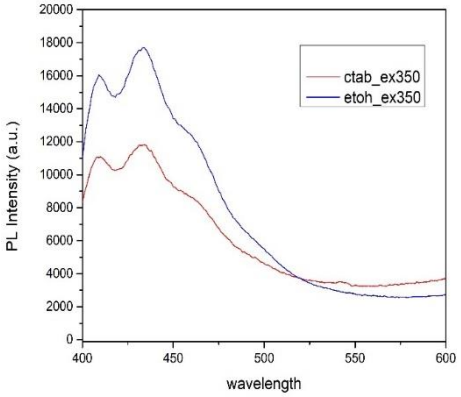


Figure 24: CTAB_ec350

Shown in the following figures are two types of graphs relevant to the PL and PLE spectroscopy, respectively; these two techniques are commonly adopted to study the optical-properties-of-materials.The PLE spectrum plots photoluminescence intensity versus excitation wavelength. In this case the excitation wavelength was scanned while monitoring the emission at 435 nm. Peaks in this spectrum indicate that those wavelengths which the material is successfully absorbing light and is producing photoluminescence at the observed emission wavelength, 435 nm.
This graph depicts the photoluminescence intensity varied with wavelength under two different environmental conditions. Changes in the shape and intensity of the peak can carry information about the interaction of the substance with the surrounding medium.

The PLE spectrum gives the effectiveness with which the material absorbs light at different wavelengths, so as to emit at 435 nm. Peaks show strong absorption at particular excitation wavelengths. You can thus compare the PL spectra of the substance in two different media so as to know how the material environment may influence its photoluminescence properties. Shifts in peak positions and intensities due to medium interactions allow for information to be extracted on changes in the electrical environment and efficiency of the photoluminescence.
IT has some morphological band gap because there is a mixture of some oxygen group in this te material. The two graphs also show that there are not such high peaks. So, it has a morphological band gap but not such as any optical properties.

Dielectric Measurement &Analysis:

Evaluating the electrical characteristics of insulating (dielectric) materials is known as dielectric measuring. Among these characteristics is the material's capacity to absorb and release electrical energy in the presence of an electric field. Dielectric testing measures permittivity (ε'), dielectric loss (ε"), and loss tangent (tan δ), which are the three main parameters.



Figure 25: Dielectric measurement device

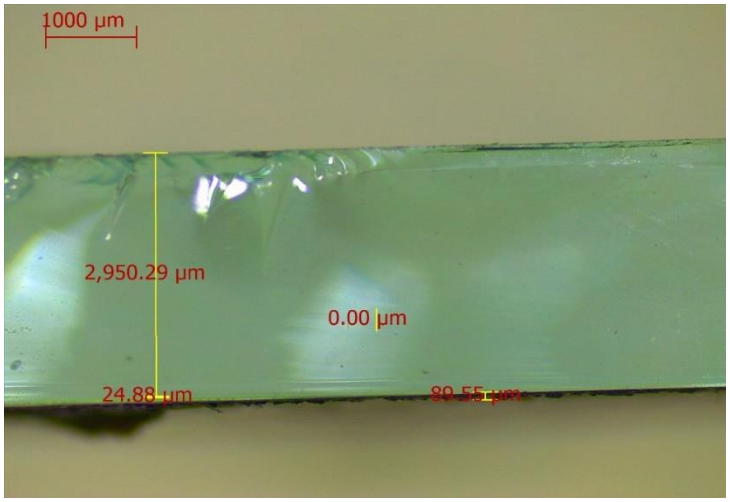


Figure 26: Image of the device from upwards

From this image we can analysis the thickness of the material on the device. Which is symbolized as (d) = 89.55 micrometre



Figure 27: Image of the device from microscope

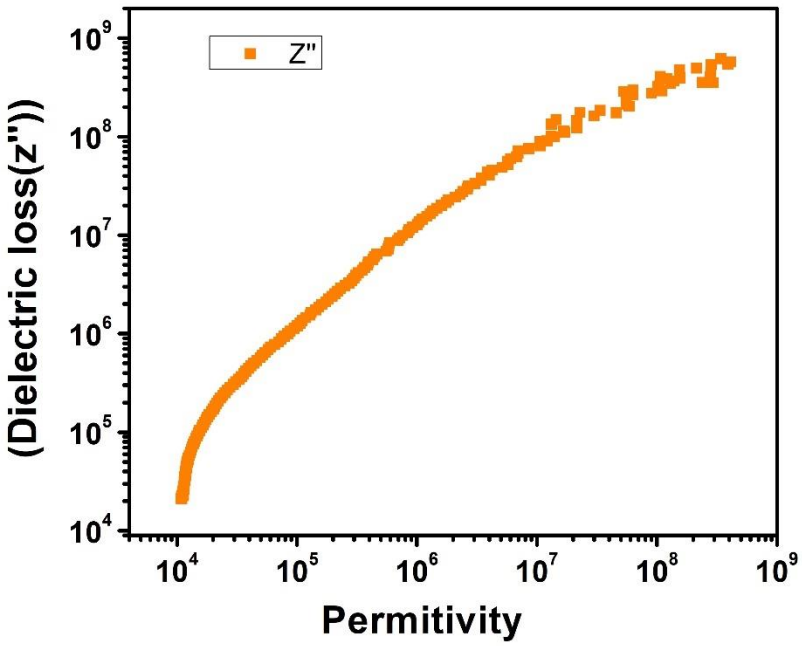


Figure 28: Dielectric graph

The graph you have sent plots the dielectric loss with respect to permittivity for a certain material. This is often the kind of graph used for analyzing a certain material when dielectric spectroscopy was done for the material's properties. The explanation, interpretation, and meaning of the graph are given below.

Plotting shows that with an increase in permittivity, there is a corresponding increase in dielectric loss. This means that the heat energy released is directly proportional to the ability of the material to store electrical energy. The values of permittivity (x-axis) and dielectric loss (y-axis) run several orders of magnitude, thereby indicating that the values for both parameters are very well spread out. Such measurements in dielectrics are performed so that the response of materials may be well characterized for different conditions or over a wide frequency window.
The substance does show a trend for higher dielectric losses whenever the permittivity is higher. This may be attributed to the fact that the material contains more polarizable entities or dipoles within the material. These assist in the mechanisms of energy dissipation and storage. The dielectric behavior usually varies in relation to the frequency of the electric field that is put across the substance. With the lower frequency, there is more time for the alignment of material dipoles with the electric field, which

would increase permittivity and therefore dielectric loss from more severe relaxation processes. The dipoles are not able to align as quickly at high frequencies, which results in a decreasing permittivity and dielectric loss. Such dependencies may be shown if the measurements were taken at various frequencies on a plot.
The graph carries important information regarding the dielectric behavior of the material. From this relationship between permittivity and dielectric loss, quite a lot of useful data is obtained from the graph concerning how the material will effectively store and dissipate electrical energy. This piece of information forms the basis of design and optimization within specific application areas in electronic and energy systems.

Scanning Electron Microscope Analysis (SEM):

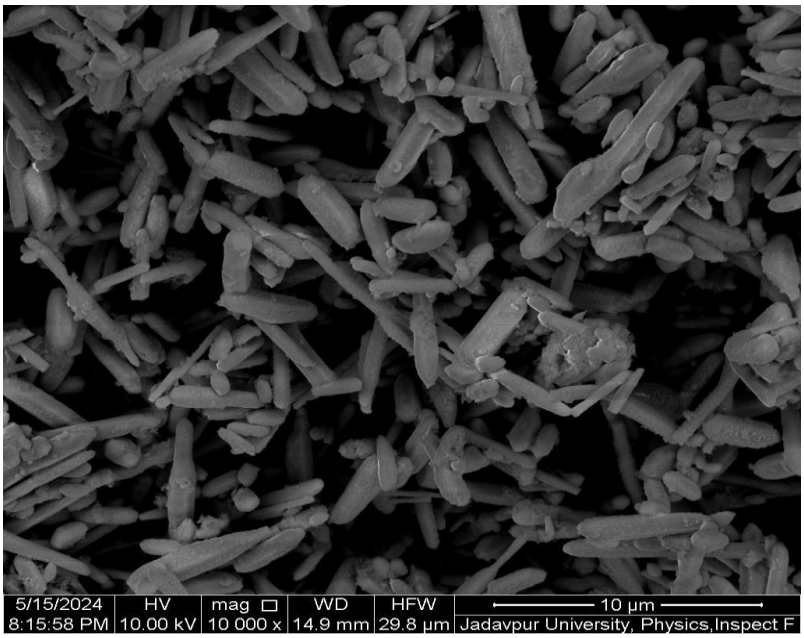


Figure 29: SEM 4 hrs

Uploaded image looks like a technical report on the dielectric behavior of a material with a focus on the use of SEM in analyzing the material's microstructure. The microstructure of the material after four hours of processing can be observed in the following SEM images. The scale bar of the images shows the dimension of items under observation:20µm.
The caption describes the importance of the understanding of the behavior of materials in terms of permittivity and dielectric loss. Such behavior understanding is most important in application domains like electronics and energy systems, where materials

are expected to store electrical energy effectively and then release it efficiently. Here, with the SEM analysis of material, one will be able to relate some structural features to the functionality of a material with regard to storing and releasing electric power. This enables the material to be optimized so that it may be used in electrical components, like insulators, capacitors, and so forth.

SEM picture shows the particles in an elongated or rod-shaped form lying in a dense cluster. Such a morphology may indicate the material to be crystalline or such that it is ordered. The particles may have been processed in such a way to make them all roughly the same because there is a remarkable uniformity among the particles. The notation "4 hrs" refers to the time in which the material was subjected to a certain treatment insomuch that it affected the type of final microstructure, therefore sintering, heating, chemical processing etc.
SEM is frequently employed to measure particle size distributions, aspect ratios, and other structural features which can be quantitatively related to dielectric performance. The surface area, grain size and crystallinity of this material - all properties that can have an impact on dielectric performance - may have been influenced by the duration of its processing.

Provide the detailed material information or experiment data, and I can help to investigate further into how these microstructural features would affect its dielectric behavior in a given application.

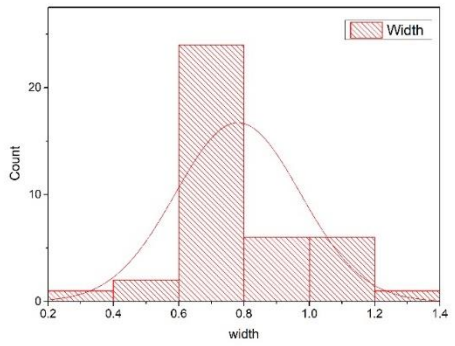


Figure 30: Histogram Plot (Width)

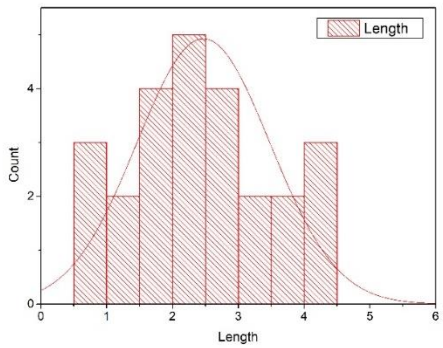


Figure 31: Histogram Plot (Length)

Width Plot (Left): This plot shows how the width values are distributed. The width values that frequently fall inside specific ranges (bins) are displayed by the bars. Since most width values are concentrated in the range of 0.6 to 0.8, the majority of dat a points have widths within that range. A continuous estimate of the data's probability density is given by the smooth curve that crosses the histogram. Unlike a histogram, which only uses discrete bins, this method smoothes the data to re veal the underlying distribution more clearly.

In this instance, the KDE peaks close to the histogram's (about 0.7) area.

The width data shows a unimodal distribution (one peak) with a centering at 0.7. This implies that, around this central value, the widths are rather constant. At the extremes (lower than 0.6 and greater than 1.0), there are fewer observations.

Length Plot (Right): Compared to the width, the frequency of the length data is scattered over a larger range. In comparison to the width data, the distribution appears more dispersed, and the peak frequency is centred around 2.5–3.0. The histogram's swings are reduced by the KDE, which also displays a distribution that is somewhat bell-shaped and centred around 2.5–3.0. There is a faint bimodal characteristic, suggesting that the data may contain two subgroups. Compared to the width data, the length data exhibits greater fluctuation. Although there is evidence of some dispersion at the extremes

(smaller and larger lengths), suggesting a wider spread or variance in lengths, the central values are roughly 2.5–3.0.

Overall Analysis:

The distribution of the width data is tighter and more consistent than that of the length data. Greater variability is seen in the length data, which may indicate the existence of several subgroups within the distribution (possible bimodality).

These features could point to variations in the production method or measurement setup for the two parameters (width vs. length).

In the event that this pertains to a material or physical investigation, the distributional variations may be the result of different production methods or ambient influences on the dimensions.

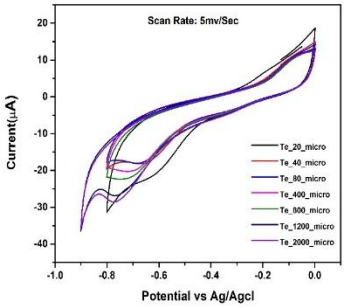
Cyclic Voltammetry Analysis (CV):

CV was utilized in the study of the electrochemical property of the Te sensor toward H2O2. The performance of Te fabricated from Acetate-based IL bath at various applied overpotentials has been were analyzed in deoxygenated phosphate buffer (PB; pH 7). It shows CV plots of Te synthesized at different OPD in argon saturated PB at scan rate of 40 mV/s. Apparently redox process involved in the oxidation and subsequent reduction of TeNPs can be observed. According to the CV measurements, the mechanism of sensing which involves peak pair TeO2/Te adsorbed over FTO can be explained as follows.

$$\mathbf{Te + 2H_2O \leftrightarrow TeO_2 + 4H^+ + 4e^-} \qquad \mathbf{(1)}$$

$$\mathbf{TeO_2 + 4H^+ + 4e^- \leftrightarrow Te + 2H_2O + 2O_2} \qquad \mathbf{(2)}$$

It can be noticed that TeNPs modified FTO reduces the red/x potential of Te at pH 7. The sensing mechanism involves a four-electron transfer process. Further, in order to determine the dynamic characteristics of Te electrodes, CV were recorded at different scan rates in the potential range −1.20 to + 1.50 V (Vs Ag/AgCl).



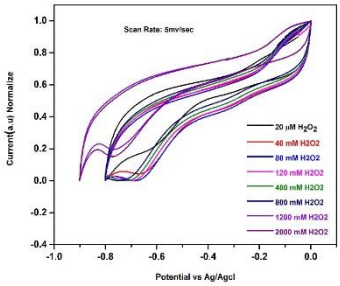


Figure 32: CV plot for 5mv/Sec **Figure 33: CV plot for 5mv/Sec (Normalize)**

The two graph in image represent Cyclic Voltammetry plot in a scan rate 0f 5mv/Sec. In left graph the various lines correlate to various "Te_micro" values, which could be indicative of various Te (tellurium) concentrations or experimental setups. In right graph the graph's lines represent different H2O concentrations, indicating that it might be comparing the effects of different H2O concentrations on cyclic voltammetry behaviour.

To enable comparison across various experimental circumstances (presumably H2O2 concentrations), the *right graph* displays the normalized current while the *left graph* displays the raw current values during the CV analysis.

Left Graph (Raw Current vs. Potential):

The absolute or raw current levels measured during the CV experiment are plotted on this graph. The amount of electron flow in response to the applied potential (voltage) is reflected in the current. This range, which is roughly between -40 µA and +20 µA, demonstrates notable variations in current under various circumstances (probably as a result of changes in the material size, Te_micro). The numerous conditions denoted by the various curves, such as "Te_20_micro," "Te_40_micro," etc., are represented. These could be attributed to variations in the composition of the material or in the sizes of the Te particles, which are affecting the current response.The current response fluctuates for every circumstance, suggesting that as the potential changes, new electrochemical behavior (such as redox activity, capacitance, and other electrochemical features) would occur.

The electrochemical characteristics can be inferred to be influenced by the differences in current between curves under various sample circumstances. Greater peaks or

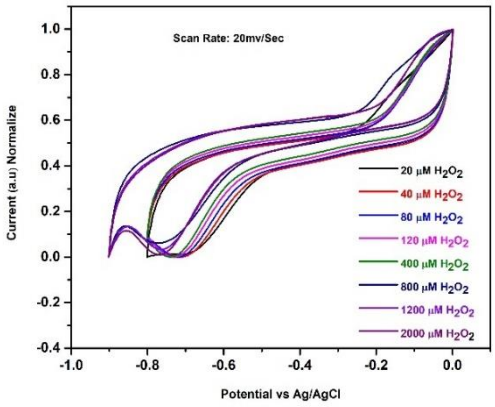
variations in the peaks indicate distinct electron transport mechanisms, which are essential to comprehending the functionality of the material.

Right Graph (Normalized Current vs. Potential):

This graph normalizes the current, which means that in order to bring all of the curves into a same scale, the current values have been modified by a specific factor (such as dividing by the maximum current, surface area, or other scaling variables). The practice of normalization aids in eliminating variations in current that result from variations in the concentrations or quantities of material utilized. Rather, it draws attention to the inherent characteristics of the materials, which lend themselves to easier comparison.

As indicated by the legend, the curves now depict various $H2O_2$ (hydrogen peroxide) concentrations. This implies that the experiment examined the relationship between the CV response and $H2O_2$ concentration, Because the current is normalized, variations in absolute current levels do not distort the graph, which highlights how the form and position of the peaks vary across different H2O2 concentrations.

This aids in comprehending how the material's intrinsic characteristics, such as catalytic efficiency, reaction kinetics, or adsorption phenomena, alter in response to external influences (such as $H2O_2$ concentration).



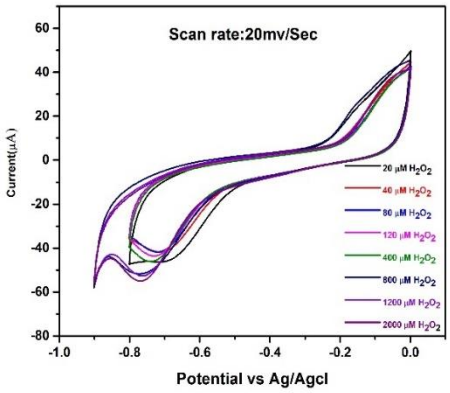


Figure 34: CV plot for 20mv/Sec **Figure 35: CV plot for 20mv/Sec (Normalize)**

In this new image, the two graphs both show CV plots at a higher scan rate of 20 mV/sec. This graph presents a normalized comparison of the effects of various H2O3 concentrations on the electrochemical behaviour. Here, relative changes—like modifications to the redox peaks and the CV curve's general shape—are the main focus. Normalization removes the effect of absolute material amounts and emphasizes intrinsic variations, such as catalytic activity, reaction kinetics, or other electrochemical

features.

The graph illustrates the absolute current values and highlights the ways in which varying Te_micro conditions—possibly due to variations in material composition, size, or thickness—affect the overall current. Because larger or more conductive materials will provide higher currents, overall performance is the important factor here. This graph highlights how the material's redox behavior is affected by different H2O2 concentrations. Different interactions between the material and $H2O_2$ at different concentrations probably cause the CV curves to alter in shape. These interactions may have an impact on the redox potential, the number of active sites, or the reaction kinetics.

The effect of various material sizes or concentrations is displayed on the right graph (Te_micro). Higher surface area or larger size materials will probably exhibit higher currents, indicating higher levels of electrochemical activity. Variations in the peak height and position can also be a sign of different electron transfer mechanisms' levels of efficiency.

Compared to the first image, which employed a slower scan rate of 5 mV/sec, the greater scan rate of 20 mV/sec in both graphs should generally result in faster electron transfer kinetics being detected and could provide new insights. Faster electrochemical processes, including catalytic reactions or adsorption/desorption phenomena, are frequently highlighted by the faster scan rate.

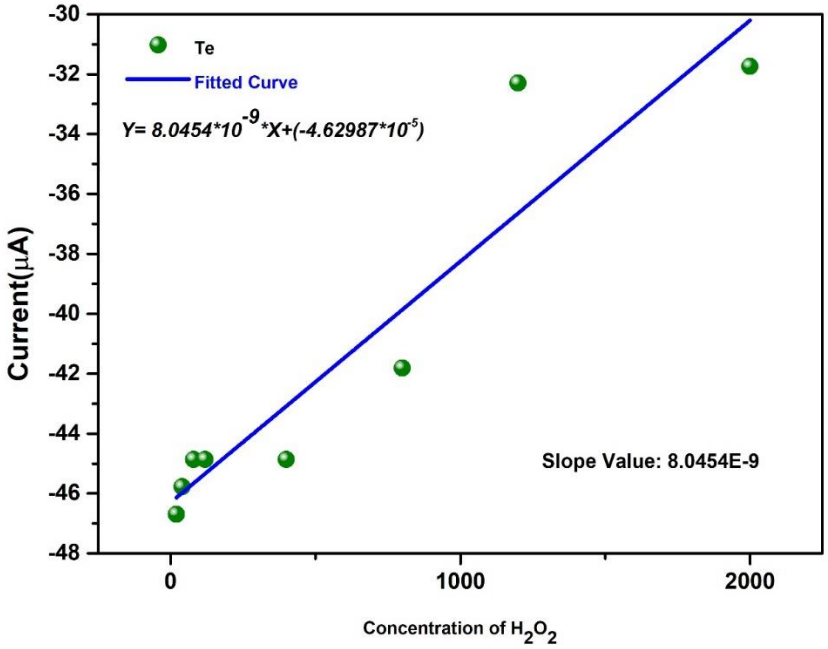


Figure 36: Sensitivity

The graph shows the relation of the H_2O_2 concentration and electrical current in microamperes(μA).

The experimental data showing the current as a function of H_2O_2 concentration is represented by the green circular points. The blue line represents a fitted curve applied to the data.

This is a linear fit, which suggests that the current and H_2O_2 concentration relationship is relatively linear in the given range. -This slope represents the rate of variation of current with respect to changes in H_2O_2 concentration.

In case the H_2O_2 concentration increases, the current decreases along with it, moving towards -30 μA. The linear fit is positive between H_2O_2 concentration and electrical current.

This graph will likely indicate a sensor's sensitivity towards the changes in H_2O_2 concentration, where the varied currents change according to changes in H_2O_2.

❖ Conclusion:

Tellurium nanorods underpin a novel, low-cost, non-enzymatic H2O2 sensor. TeNR-based non-enzymatic H2O2 sensors were made using an economically effective electrochemical method. The effects of deposition potential on nanostructured Te film phase development, morphology, and electrochemical characterization have been examined. Field emission scanning electron microscopy, X-ray diffraction, Raman, and Uv-Vis spectroscopy examined the GC surface's nanostructured Te layers. Cyclic voltammetry (CV) and chronoamperometry (CA) were used to evaluate the TeNPs/GC sensor's electrocatalytic performance in phosphate buffer with and without H2O2. TeNRs/GC showed exceptional electrocatalytic H2O2 reduction at -0.7 V.

The 5-second amperometric reaction time sensor offers excellent selectivity and stability. The current study suggests using TeNPs/FTO to measure H2O2 in samples.The low-cost, single-pot hydrothermal technique successfully produces tellurene. As prepared, Te is sensitive. Te was spin-coated layer by layer on chemically etched FTO. We investigated because the material was equally spread across the FTO glass layer. Measurement of the dielectric shows a high voltage gain. High aspect ratio 2D morphologies have considerable potential for flexible electronics, photodetectors, sensors, and thermoelectric devices because to their very anisotropic behavior in high carrier mobility and photoconductivity.

Most of these materials' potential properties—including stability and performance under original conditions—are unreached due to scalable and regulated manufacture. Future attempts to stabilize synthesis and research novel device topologies should unlock Te 2D rod-like structures' full potential. Further study and analysis of such materials may progress materials science and nanotechnology, opening up new high-tech areas.

Reference:

(1) Mani, V.; Shanthi, S.; Peng, T.-K.; Lin, H.-Y.; Ikeda, H.; Hayakawa, Y.; Ponnusamy, S.; Muthamizhchelvan, C.; Huang, S.-T. Real-time quantification of hydrogen peroxide production in living cells using NiCo2S4@CoS2 heterostructure. Sensors Actuators B Chem.2019, 287, 124−130.

(2) Waldiya, M.; Bhagat, D.; R, N.; Singh, S.; Kumar, A.; Ray, A.; Mukhopadhyay, I. Development of highly sensitive H2O2 redox sensor from electrodeposited tellurium nanoparticles using ionic liquid. Biosensor. Bio electron. 2019, 132, 319−325.

(3) Manikandan, M.; Dhanuskodi, S.; Maheswari, N.; Muralidharan, G.; Revathi, C.; Rajendra Kumar, R. T.; Mohan Rao, G. High-performance supercapacitor and non-enzymatic hydrogen peroxide sensor based on tellurium nanoparticles. Sens. Bio-Sensing Res. 2017,13, 40−48.

(4) Zhu, L.; Zhang, Y.; Xu, P.; Wen, W.; Li, X.; Xu, J. PtW/MoS2 hybrid nanocomposite for electrochemical sensing of H2O2 released from living cells. Biosens. Bioelectron. 2016, 80, 601−606.

(5) Suchand Sandeep, C. S.; Samal, A. K.; Pradeep, T.; Philip, R. Optical limiting properties of Te and Ag2Te nanowires. Chem. Phys. Lett. 2010, 485, 326−330.

(6) (19) Xi, G.; Wang, C.; Wang, X.; Qian, Y.; Xiao, H. Te/Carbon and Se/Carbon Nanocables: Size-Controlled in Situ Hydrothermal Synthesis and Applications in Preparing Metal M/Carbon Nanocables (M = Tellurides and Selenides). J. Phys. Chem. C 2008, 112(4), 965−971.

(7) Mayilmurugan, M., Rajamanickam, G., Perumalsamy, R., & Sivasubramanian, D. (2022). Nickel cobalt telluride nanorods for sensing the hydrogen peroxide in living cells. *ACS omega*, *7*(17), 14556-14561.

(8) Gao, M., Wang, X., Hong, Y., Shi, Y., Wang, D., Fang, D., ... & Wei, Z. (2019). One-Pot Hydrothermal Synthesis of Thin Tellurene Nanosheet and Its Formation Mechanism. *Journal of Nanomaterials*, *2019*(1), 5715291.

(9) Li, C., Gao, F., Wang, Y., Zhao, L., Li, H., & Jiang, Y. (2022). Advances of bioactive tellurium nanomaterials in anti-cancer phototherapy. *Materials Advances*, *3*(16), 6397-6414.

(10) Liu, Z., Li, S., Yang, Y., Hu, Z., Peng, S., Liang, J., & Qian, Y. (2003). Shape-controlled synthesis and growth mechanism of one-dimensional nanostructures of trigonal tellurium. *New Journal of Chemistry*, *27*(12), 1748-1752.

(11) Zhu, H., Fan, L., Wang, K., Liu, H., Zhang, J., & Yan, S. (2023). Progress in the Synthesis and Application of Tellurium Nanomaterials. *Nanomaterials*, *13*(14), 2057.

(12) Deckoff-Jones, S., Wang, Y., Lin, H., Wu, W., & Hu, J. (2019). Tellurene: a multifunctional material for midinfrared optoelectronics. *ACS Photonics*, *6*(7), 1632-1638.

(13) Grillo, S., Pulci, O., & Marri, I. (2022). Evolution of the electronic and optical properties of meta-stable allotropic forms of 2D tellurium for increasing number of layers. *Nanomaterials*, *12*(14), 2503.

(14) Wang, D., Yang, A., Lan, T., Fan, C., Pan, J., Liu, Z., ... & Koratkar, N. (2019). Tellurene based chemical sensor. *Journal of Materials Chemistry A*, *7*(46), 26326-26333.

(15) Cui, Heping, et al. "Tellurene nanoflake-based NO2 sensors with superior sensitivity and a sub-parts-per-billion detection limit." *ACS Applied Materials & Interfaces* 12.42 (2020): 47704-47713.

(16) Waldiya, M., Bhagat, D., Narasimman, R., Singh, S., Kumar, A., Ray, A., & Mukhopadhyay, I. (2019). Development of highly sensitive H2O2 redox sensor from electrodeposited tellurium nanoparticles using ionic liquid. *Biosensors and Bioelectronics*, *132*, 319-325.

(17) Sári, D., Ferroudj, A., Semsey, D., El-Ramady, H., Brevik, E. C., & Prokisch, J. (2024). Tellurium and Nano-Tellurium: Medicine or Poison?. Nanomaterials, 14(8), 670.

(18) Sahoo, T., Sahu, J. R., Panda, J., Kumari, N., & Sahu, R. (2020). Application of Two-Dimensional Monoelements-Based Material in Field-Effect Transistor for Sensing and Biosensing. Monoelements: Properties and Applications, 119-148.

(19) Jiang, J., Zhang, R., & Wu, W. (2023). Wearable Sensors Based on Atomically Thin P-Type Semiconductors. Advanced Materials Technologies, 8(18), 2300517.
(20) Chen, W., Cai, S., Ren, Q. Q., Wen, W., & Zhao, Y. D. (2012). Recent advances in electrochemical sensing for hydrogen peroxide: a review. Analyst, 137(1), 49-58.